NED UNIVERSITY

JOURNAL OF RESEARCH

Vol. VI No. 1

JUNE 2009

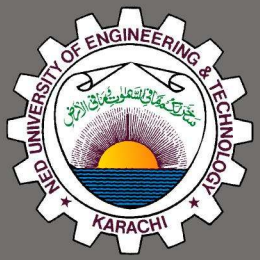

NED UNIVERSITY OF ENGINEERING AND TECHNOLOGY

NED UNIVERSITY JOURNAL OF RESEARCH

Editor

Dr. Muhammad Masood Rafi
Professor
Department of Civil Engineering
NED University of Engineering & Technology, Karachi-75270, Pakistan
Tel: +92(-0)21 9261261-8 Ext.2277, Fax: +92(0)21 9261255
Email: NED-Journal@neduet.edu.pk

International Editorial Advisory Board

Dr. Sahibzada Farooq Ahmad Rafeeqi
Professor & Dean,
Faculty of Civil Engineering & Architecture,
NED University of Engineering & Technology, Karachi-75270, Pakistan
Email: deancea@neduet.edu.pk

Dr. Nazim Uddin Qureshi
Professor & Dean, Faculty of Mechanical & Manufacturing Engineering,
NED University of Engineering & Technology, Karachi-75270, Pakistan
Email: deanmme@neduet.edu.pk

Dr. Talat Altaf
Professor & Dean, Faculty of Electrical & Computer Engineering,
NED University of Engineering & Technology, Karachi-75270, Pakistan
Email: deanece@neduet.edu.pk

Dr. Mahmood Khan Pathan
Professor & Dean, Faculty of Science, Technology & Humanities,
NED University of Engineering & Technology, Karachi-75270, Pakistan
Email: deanish@neduet.edu.pk

Dr. Muhammad Tufail
Professor and Chairman
Department of Industrial and Manufacturing Engineering
NED University of Engineering & Technology, Karachi-75270, Pakistan
E-mail: cid@neduet.edu.pk

Dr. Omar S. Baghbra Al-Amoudi
Professor & Assistant Dean, Continuing Education Deanship of Education
King Fahd University of Pertoleum & Minerals
Dhahran 31261, Saudi Arabia
Email: amoudi@kfupm.edu.sa

Dr. Rizwanuddin
Professor, Department of Nuclear, Plasma & Radiological Engineering
University of Illinois at Urbana Champaign
Urbana, IL-61801, USA
Email: rizwan@uiuc.edu

Dr. Afaq Ahmed
Associate Professor
Department of Electrical Engineering
Sultan Qaboos University
P.O.Box 33, Al-Khod
Sultanante of Oman
Email: afaq@squ.edu.om

Dr. Sarosh Hashmat Lodi
Professor & Chairman
Department of Civil Engineering
NED University of Engineering & Technology, Karachi-75270, Pakistan
Email: civilchr@neduet.edu.pk

Dr. Khalid Aziz
Professor of Energy Resources Engineering
Stanford University
65 Green Earth Sciences Building
367 Panama Street
Stanford, CA 94305-2220, USA
Email: aziz@Stanford.EDU

Dr. Abdul Fazal M. Arif
Associate Professor
Department of Mechanical Engineering
King Fahad University of Petroleum & Minerals
Dhahran-31261, Saudi Arabia
Email: afmarif@kfupm.edu.sa

Dr. Shakil Akhtar
Head IT Department
Clayton State University
2000 Clayton State Blvd
Morrow, GA 30260-0285
USA
Email: sakhtar@ieee.org

Professor Alan Michette
Department of Physics
King's College, London
Strand, London WC2R 2LS
UK
Email: alan.michette@kcl.ac.uk

Dr. Syed Tanvir Wasti
Professor Emeritus
Department of Civil Engineering
Middle East Technical University
06531 Ankara/Turkey
Email: stwasti@ce.metu.edu.tr

Dr. Tasneem Pervez
Associate Professor and Chair
Department of Mechanical and Industrial Engineering
Sultan Qaboos University
P.O.Box 33, Al-Khod
Sultanante of Oman
Email: tasneem@squ.edu.om

Dr. Bign-Zhao Li
Department of Mathematics
School of Science
Beijing Institute of Technology
China
Email: li_bingzhao@bit.edu.cn

Dr. Ian M. May
Professor of Civil and Offshore Engineering
Heriot-Watt University
Edinburgh EH 14 4AS
Scotland, UK
Email: I.M.May@hw.ac.uk

Dr. Ali A Minai
Associate Professor
Complex Adaptive Systems Lab
Department of Electrical & Computer Engineering
University of Cincinnati
Cincinnati, OH 45221-0030, USA
Email: minai_ali@yahoo.com

Dr. Shuaib Ahmad
President
Zenith International Ltd
7A/I, 4th North Street
Phase I, DHA, Karachi, 29170
Pakistan
Email: sahmad1234@gmail.com

NED UNIVERSITY
JOURNAL OF RESEARCH

Published by NED University of Engineering & Technology, Karachi-75270 – Pakistan

Vol. VI No. 1 2009 ISSN 1023-3873

The NED University Journal of Research is a biannually, refereed Journal. It is distributed internationally. Principal emphasis is in the area of Engineering Disciplines. All rights reserved in favour of NED University of Engg. & Tech., Karachi.

Address For Correspondence:
Dr. Muhammad Masood Rafi
Professor
Department of Civil Engineering
NED University of Engineering & Technology,
Karachi-75270, Pakistan
Tel: +92(-0)21 9261261-8 Ext.2277,
Fax: +92(0)21 9261255
Email: NED-Journal@neduet.edu.pk

Annual Subscription:
Rs 1000 (Pakistan), US$ 100.00 (Rest of the world)
Single Issue : Rs 500

Editor's Note

The issue of the NED University Journal of Research in hand is based on the changed format as approved by its members of International Advisory Board. All these changes are in line with our axiom that we shall continuously strive for improvement. The journal has a new title cover which has been redesigned to make it compatible in style with other world-wide scientific journals and magazines.

Other changes, as approved by the International Advisory Board, include a short biography, along-with a photograph of authors of accepted papers. This will provide an opportunity to the readers to learn about the authors, their academic background and their work. Secondly, a short history of review process of the accepted paper will be provided to give an idea of the duration a manuscript took for its final acceptance. Moreover, it has been decided that the journal will be publishing discussions on published original research papers from readers. It has further been approved by the Board to acknowledge the services of the reviewers by publishing their names in the December issue of the journal each year. It is hoped that these changes would be welcomed by the readers.

This issue contains three original research papers which have been approved after going through the approved peer review process. These papers are in the areas of Remote Sensing and Geographic Information Systems, Bio Diesel Engine Testing and Transportation Engineering/Travel Demand Modelling. Discussions from readers on these papers are very much welcome and will be published in June 2010 issue of the Journal, if received within stipulated time period. In line with the publication policy, two papers having significant value for the academics in Pakistan are being reproduced after taking due permission from the publishers of respective journals.

I hope that the readers will not only appreciate research papers but also the changes made in the journal style. I indeed look forward for comments from the readers as these are the prime source of improvements for future.

Editor

LAND DEVELOPMENT ASSESSMENT ON THE PRESERVED AL SAMMALYAH ISLAND/UAE USING MULTI-TEMPORAL AERIAL PHOTOGRAPHS AND GIS

Salem M. Issa[1]

ABSTRACT

The main objective of this study is to apply the most appropriate change detection techniques to assess land development achievements on Al Sammalyah Island, off the coast of Abu Dhabi, United Arab Emirates capital city. This was accomplished by mapping trajectory of land cover change of the whole island between 1999 and 2005. Another objective was to assess the level of development that occurred on the island and the level of change in the local environment. Available historical large scale aerial photographs from the late nineties to the most recent 2005 were used for the multi-temporal study. Geographic information systems (GIS) layers were created by on-screen digitizing of corrected and co-registered images. A GIS overlay analysis combined with post classification change detection method analysis schema was adopted. Results of the current study demonstrate intense land development occurring on the AL Sammalyah Island; vegetation cover extent has increased from 3.742 km^2 (1.44 miles^2) in 1999 to 5.101 km^2 (1.97 miles^2) in 2005 that corresponds to 36.3% increase over this period. The study also shows that this increase in vegetation extent is mostly attributed to the increase in mangrove planted areas alone with an aerial increase from 2.256 km^2 (0.87 miles^2) in 1999 to 3.568 km^2 (1.38 miles^2) in 2005, an increase of 58.2% in seven years.

Keywords: Change detection, Abu Dhabi, UAE, remote sensing, aerial photographs, GIS, land cover

1. INTRODUCTION

Investments generated from oil exports have resulted in an extensive development of the United Arab Emirates (UAE). This development is manifested in the rapid change in landscape, settlements, and infrastructure. In arid environments, where fragile ecosystems exist, the land cover change often reflects the most significant impact on the environment due largely to excessive human activities. Remote sensing (RS) and geographic information systems (GIS) are powerful tools to trace and evaluate land cover changes, thus play a major role in emphasizing land development demonstrating its impact on the arid environment and the local society [1-4].

This paper covers the first phase of a research project for building a GIS system for AL Sammalyah Island. The island has witnessed high rates of change in land use in the past few years, especially after the establishment of the Department of Environmental Research (DER) in 1996, which emphasized an environmental management approach. The mandate of the DER is: "to protect and

[1]*Assistant Professor, Department of Geology, UAE University, Ph. +971 (0) 50 7132865, Fax. +.971(0) 3 7671291, Email salem.essa@uaeu.ac.ae*

Manuscript received on 29th September 2008, reviewed and accepted on 17th March 2009 as per publication policies of the *NED University Journal of Research*. Pertinent discussion including authors' closure will be published in June 2010 issue of the Journal if the discussion is received by 30th November 2009.

Salem Issa received his PhD in RS/GIS from the University of Leicester, UK. He has been working as a faculty member in the Geology Department at the United Arab Emirates University since 2002. He teaches Remote Sensing/GIS and related topics. He has published a number of distinguished research papers with a focus on studying and modelling environmental issues using remote sensing and GIS related to the UAE and the region.

develop the wildlife and to preserve and develop the ecosystem on the Island". At this stage of the project we intend to analyze the change that occurred in the island during the past decade by using multi-scale, multi-temporal and high resolution aerial photographs. The integration of multi-scale aerial photographs and GIS is of paramount importance in change detection studies, and has a high cost to benefit ratio. The outcome of this study will contribute to the building of a GIS database for sustainable development and management of the island in the long term [5].

Objectives of the study are:

1) To apply most appropriate change detection techniques for land development assessment using archived high resolution historical aerial photographs;
2) To apply GIS overlay functions to map temporal and spatial trajectory of the change; and
3) To evaluate indicators of the rapid development in the construction and infrastructure works, and the rehabilitation of the island.

2. BACKGROUND

Change detection is defined as the process of identifying differences in the state of an object or phenomenon by observing it at different times. The basic principle in using remotely sensed data for change detection is that changes in the objects of interest will result in changes in reflectance values or in local textures, which are separable from changes caused by other factors such as differences in atmospheric conditions, illumination and viewing angles, and soil moistures [6-7]. Numerous works have been reported in these fields. However, change detection, imagery data from various dates, various sensors such as Aerial photographs, Landsat Multi-Spectral Scanner (MSS), Thematic Mapper (TM), Enhanced Thematic Mapper (ETM+), Satellite Pour L'Observation de la Terre High Resolution Visible (SPOT HRV), Indian Remote Sensing Satellite (IRS) and IKONOS are often used. It is also very common to use images with various scales and from two or more sensors [5, 8-13].

Nevertheless, little or no work has been conducted in the UAE to evaluate this change and to emphasize its environmental impact in the country. Few examples exist that focus on one or two issues. For example, the study presented by Alhameli and Alshehhi [14], produced a succession of historical images to reflect the rapid development in the whole country between 1973 and 2003. A detailed study by Yagoub [15], emphasized the extent of the change in Al Ain city between 1976 and 2000. However, there are no publications on building a GIS database for assessing development rates in the country and/or for natural resource monitoring and management similar to the "AL Sammalyah project" [14,15].

3. STUDY AREA

AL Sammalyah is located at approximately between 24° 26'10"N - 24° 28'56"N and 54° 29'22"E - 54° 34'12"E (**Figure 1**). It is situated in the Arabian Gulf, about 12 km (7.5 miles) north east of Abu Dhabi Island near Um al-Nar Island and just opposite Shati'-Al Raha beach. It is characterized by its rich ecosystems and marine life. The Island area covers about 14 km^2 (5.4 $miles^2$). Its geomorphology is characterized by a flat desert surface with small artificial sandy hills and dispersed coastal Sabkhat especially in the low lands along the shoreline. The island is characterized by its hyper arid climate. The mean annual rainfall is less than 50 mm/yr (2 in/yr), while the mean monthly temperature is above 30°C (86°F). Soil texture is dominated by sand with high salt content reaching 31.5% TSS on the surface. The salt, being mostly Chloride soluble, gives a white color to the soils of the island**,** which produces high brightness levels on satellite imagery operating in the visible portion of the EMR. However the very narrow mangrove soils surrounding the island have dark color because of the high content of organic carbon**.** The Island, particularly the mangroves (Avicenna marina), is a natural reserve containing high biodiversity that grow throughout the coastal areas of Abu Dhabi Emirate and is associated with varieties of plant communities including: Arthrocnemum macrostachyum, Seidlitzia rosmarinus, Suaeda vermiculata, and Cyperus conglomerates.

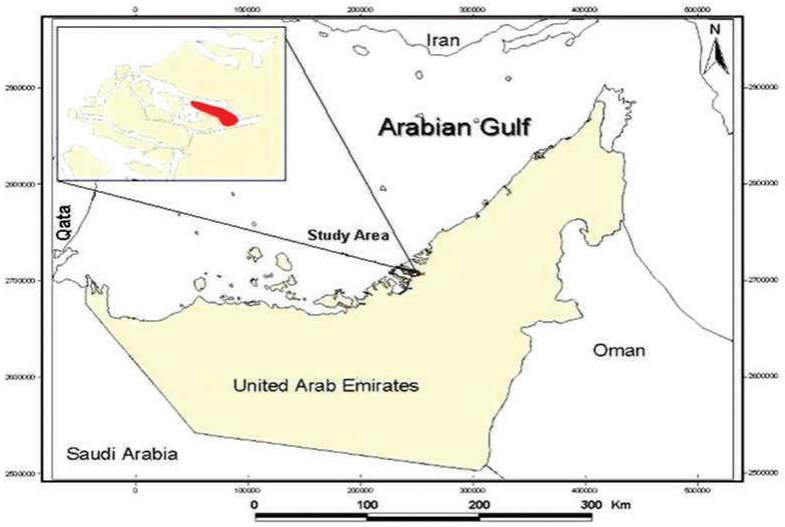

Figure 1. Location of the study area

4. DATA

Since al Sammalyah island has limited surface extent (≈14 km^2 (≈5.4 $miles^2$)), high resolution remote sensing data was the target. A time sequence of large scale aerial photographs from 1985, 1999, 2000 and 2005 was available when we started this study. Most aerial photographs have been procured from the Military Survey Department (MSD), and Abu-Dhabi Municipality. The software used in this work includes ARCGIS v9.1 software (ESRI, Redlands, CA) for vector processing, and ERDAS Imagine 8.4 for image processing. The hardware used includes PC Pentium IV 3.2 GH speed, and HP color LaserJet printers. The selection of data, used in this study was largely governed by availability and accessibility of archived data especially at the MSD archives. The selection of hardware, and software was governed by both budget limitation and UAE University/geology department's facilities.

5. METHODOLOGY

The methodology applied to this study is based on integrated GIS and remote sensing methods, with the advantage of using GIS ability to combine different source data into the change detection process. Since no major activities on the island are noticed from the mid-1980s aerial photographs, a change detection analysis between 1999 and 2005 has to be conducted. Aerial photographs from 1999 and 2005, at scales of 1:30,000 and 1:10,000 respectively, are used and a post-classification comparison method is implemented for conducting the change detection analysis [7,10,16-22]. Visual analysis method is used for image interpretation and simultaneously an on-screen digitizing is performed. Texture, shape, size and patterns of the images are used for feature identification. Precise positional accuracy, fine spatial resolution and good contrast between irregularly distributed vegetation (appearing as naturally distributed dark spots), regularly planted vegetation (appearing as dark regular rows) and dark soil with no or sparse vegetation (appearing as brown, smooth textured large continuous spots) allowed precise on-screen digitizing to be conducted. Ground truthing had been carried out at the beginning and during the study to set up the land cover classes so that recognized objects were confirmed with certitude especially that the study area is limited in surface [6, 8-10, 15].

6. RESULTS

Aerial photographs were scanned at a resolution of 1200 dpi, at the Military Survey Department. The nearest neighbour method of grey-level interpolation was applied. Pixel resolutions of 4 m (13.1 ft) and 2 m (6.6 ft) were obtained for the 1999, and for both the 2000 and 2005 aerial photographs respectively. The 2000-aerial photograph was already projected to the Universal Transverse Mercator, zone 40 (UTM) at the Military Survey Department. This image was used as a master image to register other datasets using an image-to-image registration. A minimum of 10 ground control points (GCPs) was collected for each photograph and a second degree polynomial transformation was used to project them. The total Root Mean Square (RMS) was less than 0.4

Table 1. Land cover classes used for the interpretation of the aerial photographs of 1999 and 2005.

Class number	Name of land cover class
1.	Roads
2.	Footpaths / tracks
3.	Roundabouts
4.	Water bodies
5.	Water Channels
6.	Bushes
7.	Palm trees
8.	Mangroves
9.	Buildings
10.	Break waters / bays / ports / petrol station
11.	Barren land

pixels. The resulting aerial photographs were then resampled by using ERDAS Imagine Map Interpreter Function and a final pixel resolution of 2 m (6.6 ft) was obtained for all datasets. A unified land cover classification scheme was established. Eleven land cover classes were identified in the image interpretation process (**Table 1**) and were brought into a GIS database. GIS overlay analysis was applied to extract information and map changes in land cover that had occurred on the island between these two dates.

For analysis purposes the researcher proposed the grouping of the eleven land cover classes into four different groups to facilitate results analysis and interpretation. Each group was considered as a development measure (positive or negative) on the Island. Group one is a measure of urbanization development; group two reflects greening development; group three detects land disturbance; and group four assess conservation and land reclamation development.

The 1999 and 2005 land cover maps were categorized into the following four categories:
Category 1: Roads, Roundabout, and Buildings; as a measure of urban development.
Category 2: Mangrove (near the NNE coast and in the inner parts of the island), Palm trees (along roads and as firm borders) and other trees and grasses (near the ENE coast); as a measure of forestation, agricultural activities, and environmental development.
Category 3: Barren land, Tracks and Footpaths; as a measure of desertification and land disturbance.
Category 4: Water bodies and Water Channels; as a measure of conservation and land reclamation development.

Statistics and aerial extent of land cover types and their changes are presented in **Table 2** while in **Figure 2** land cover maps reflecting the island development between 1999 and 2005 are shown.

Table 2. Land cover statistics in the study area between 1999 and 2005.

No	Class name	1999	2005	Increase	Decrease	% Change
1.	Roads (km)	21.6	26.7	5.1	-	+23.6
2.	Footpaths & tracks (km)	33.917	23.08	-	10.837	-32
3.	Roundabout (number)	2	8	6	-	+300
4.	Water bodies (km^2)	0	0.015	0.017	-	+New
5.	Water Channels (km)	20.4	23.2	2.8	-	+13.7
6.	Bushes (km^2)	1.322	1.322	-	-	0
7.	Palm trees (km^2)	0.164	0.210	0.046	-	+28.1
8.	Mangroves (km^2)	2.256	3.568	1.312	-	+58.2
9.	Buildings (km^2)	0.05	0.16	0.11	-	+220
10.	Break waters / bays / ports / petrol station (number)	3 / 1 / 2 / 1	3 / 3 / 2 /1	2	-	+29
11.	Barren land (km^2)	9.60	8.16	-	1.44	-15

1999 **2005**

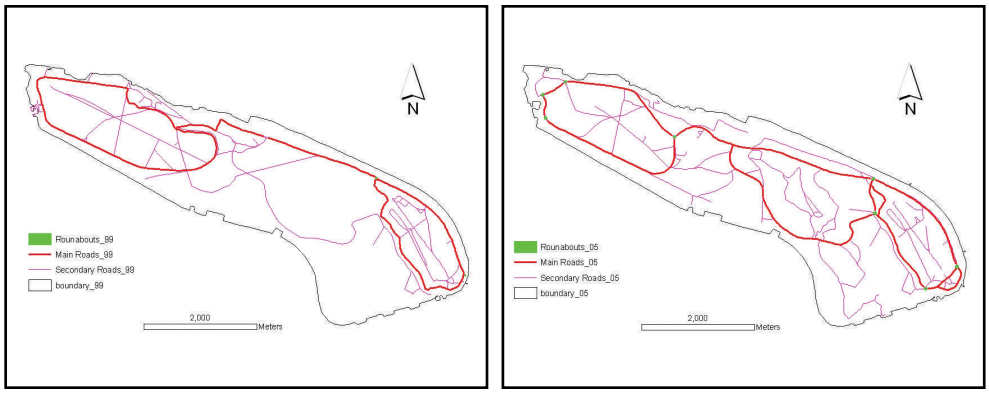

(a) Roads & Roundabouts

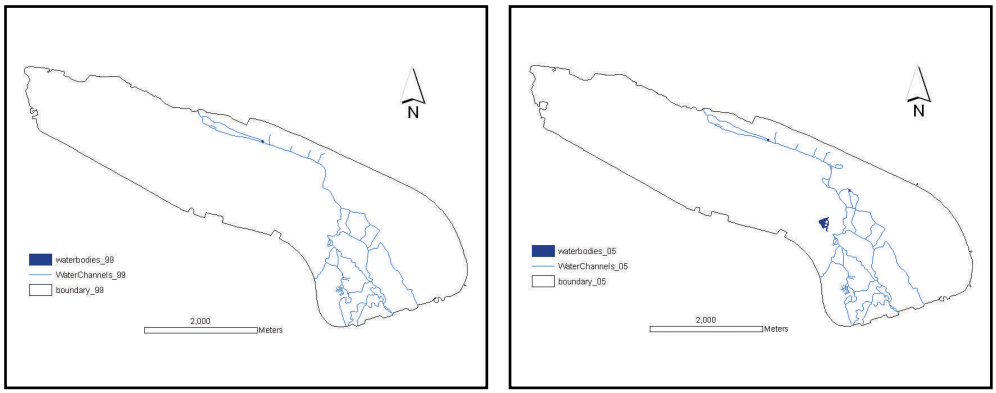

(b) Water bodies & Water channels

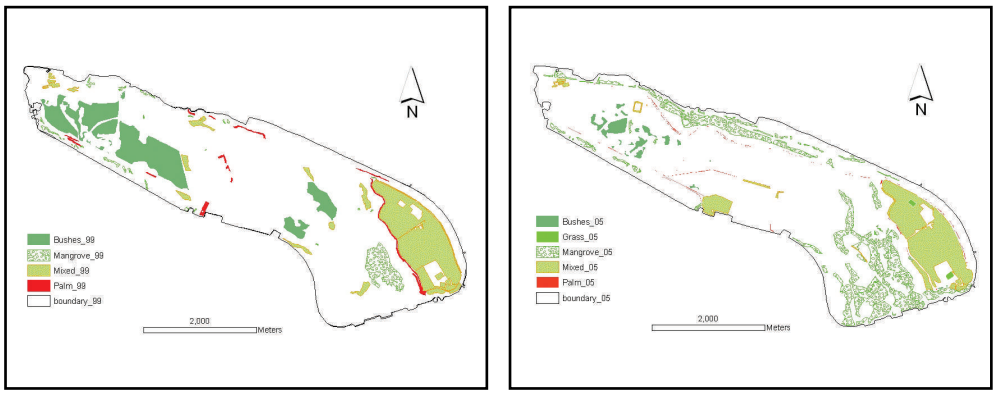

(c) Vegetation

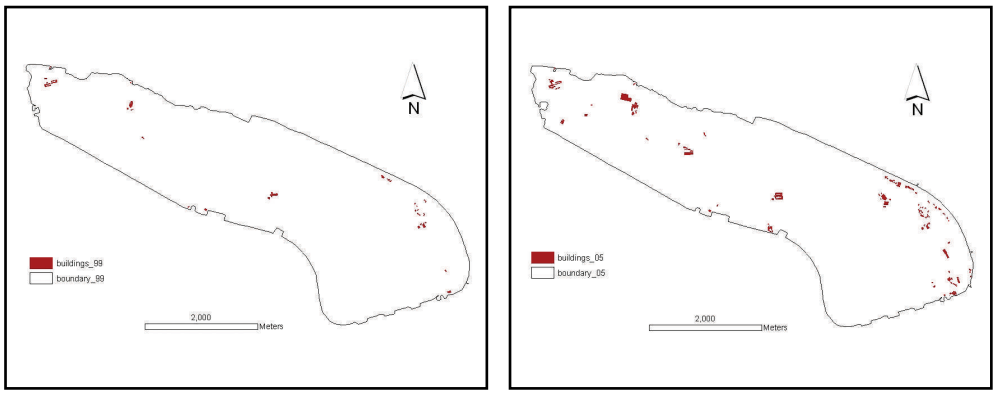

(d) Buildings

Figure 2. The 1999 and 2005 Land cover maps of main classes: (a) Roads Network; (b) Water bodies and water channels; (c) Vegetation; and (d) Buildings.

7. DISCUSSION

7.1. Urbanization: Changes in Roads, Roundabouts, and Building (1999 - 2005)

Table 2 shows that between the years 1999 and 2005 there has been an increase of 23.6%, 300% and 220% in roads length, number of roundabouts and buildings areas respectively. This high increase of the level of urbanization on the island required large amounts of investment from the managing organization, to satisfy the increased demand to build new touristic, scientific and sports facilities. Examples range from horse riding halls, Olympic shooting range, Olympic swimming pools, laboratories, green houses, offices, dormitories, and the establishment of a modern road network. These facilities are used to host increasing numbers of students from all around the country as well as researchers, and also to promote ecotourism. This is attributed to the high-level political will of H H Sheikh Sultan Bin Zayed, Chairman of the Emirates Heritage Club to transform the island from a desertified area into a well-developed reserve for protecting wild life and ecosystems and for developing ecotourism and preserving local heritage.

7.2. Forestation, Greening and Environmental Development: Changes in Vegetation Cover Extent (1999 - 2005)

The aerial extent of the cover types are presented in **Table 2**. Total vegetation cover extent has increased from 3.742 km^2 (1.44 $miles^2$) in 1999 to 5.101 km^2 (1.97 $miles^2$) in 2005; an increase of 36.3% between 1999 and 2005. The density of the vegetation has also increased, giving increase to the overall biomass production on the island. This biomass production can be quantified using vegetation indices calculated from satellite imagery and will be one of the objectives of future studies using satellite imagery. Furthermore, the increase in vegetation extent is mostly attributed to the increase in mangrove planted areas. Indeed, mangrove planted area has increased from 2.256 km^2 (0.87 $miles^2$) in 1999 to 3.568 km^2 (1.38 $miles^2$) in 2005; an increase of 58.2% in seven years. This gain in the mangrove – occupied areas has occurred on previously barren land which has been reclaimed and irrigated using sea water, hence indicating the success of procedures applied to combat desertification, enhance biodiversity and sustain the environment on the island. Mangrove is highly adapted to the conditions of the island, it is known for its high salt-tolerance, as a soil stabilizer, an ideal marine and bird habitat, and can sustain bees that give uniqueness to the mangrove honey production.

This success in increasing the extent of vegetated areas especially mangrove plantations, gives the evidences that the UAE is wisely investing in the domain of scientific research oriented at producing species that are adapted to its climatic conditions and hence increasing green areas and combating desertification locally and in the region.

7.3. Desertification and Land Disturbance: Changes in Barren Land Extent and Footpath Lengths (1999- 2005)

Barren land extent was studied as an indicator of desertification throughout the island, while tracks and footpaths lengths are used as an indicator of land disturbance and hence another indicator of desertification. **Figures 2** and **3** and **Table 2** show that there has been a decrease of 15 % in barren land areas between 1999 and 2005; while tracks and footpaths lengths have decreased by 32% between these two dates. This is another indicator of the decrease in desertification levels and the development of the ecosystems on the island during the study period. The loss in the bare and disturbed areas is due primarily to new vegetated areas (85%), urbanization (11%), and water bodies and water channels (4%).

7.4. Conservation and Land Reclamation: Changes in Water Bodies and Water Channels (1999 - 2005)

The spreading of water bodies and water channels is clear evidence of conservation and land reclamation. **Table 2** shows that there has been an increase of 13.7% in the channel networks between the two data sets, while water surfaces appear on the 2005 imagery only with a large artificial salt water lagoon of 0.015 km^2 (0.0058 miles) (**Figure 3**). Water surfaces are designed to attract migrant birds during the winter season and to develop aquatic life on the island, while channels are used to bring high-tide sea current generated water into mangrove areas.

Figure 3. Large water reservoir on the 2005 aerial photograph.

8. IMPORTANCE OF THE STUDY

The value of this study resides in building the first historical large-scale aerial photograph database for the island. The aerial coverage was not available to island managers before, because it was not considered for the public use and was kept in the archives of the MSD. Furthermore, the use of remote sensing to quantify the land use change, the development rates and the urbanization opens the door, in the country, to benefit from high resolution remote sensing imagery which can now be used for the implementation of a master plan as well as long term monitoring and management of the natural resources on the island. In addition, it provides evidence of environmental conservation and development which is being carried out on the island using indicators such as the increase in vegetation cover extent, especially salt-tolerant plants, the decrease of bare lands, and the increase in water bodies.

The study will provide opportunities to undertake future GIS-based research to conduct environmental impact studies of oil or marine pollution on the ecosystems of the island and will serve as a model of using remote sensing and GIS approach to environmental studies in the region, especially on similar protected islands.

Finally, researchers believe that this work is a first step towards developing an integrated GIS database including layers of vegetation species, vegetation density, vegetation indices, soil types, water bodies, infrastructures, and utilities to establish a GIS system for the island. The system, which will be used by managers, tourists, researchers and scientists will serve three objectives: first, as a tool for management and decision making, second to provide an on-line visualization system for monitoring and assisting in the decision making process, and third to disseminate and provide an on-line source of information regarding the island, its ecosystems and the facilities provided for the scientific community as well as the general public.

9. CONCLUSION

In early 1990s a large-scale reclamation started on the island and has been increased very rapidly since then. This has been confirmed by the decrease in bare land and by the increase in vegetated areas especially plantations of salt-tolerant mangroves and palm trees. The urbanization and the spread of water bodies is a testimony to the development of the quality of life on the island and the ecosystem.

This study was the first to be conducted on the island primarily to quantify rates of change and levels of development using remote sensing.

ACKNOWLEDGMENTS

The author is grateful to the following: (i) the Emirates Heritage Club, DER, for the financial support to carry out this work; (ii) the Research Affaires at the UAE University for their assistance and continuous support to this research; and finally (iii) Mr. Gaber Abdul Fattah for his assistance in digitizing vector data, pre-processing of aerial photos and in preparing some figures for this paper.

REFERENCES

[1] Millington A, Al-Hussein S, Dutton R. Population Dynamics, Socio-Economic Change And Land Degradation In Northern Badia, With Special Reference To The Badia Research And Development Project Area. Applied geography 1999;19:363-384.

[2] Lumbanraja JT, Syam H, Nishide A, Mahl K, Utomo M, Kimura M. Deterioration Of Soil Fertility By Land Use Changes In South Sumatra, Indonesia, From 1970 to 1990. Hydrological Processes 1998;12:2003-2013.

[3] Doran JW. Soil Health and Global Sustainability, Translating Science into Practice. Agricultural Ecosystems and Environment 2002;88:119-127.

[4] Roy PS, Tomar S. Landscape Cover Dynamics Pattern in Meghalaya. International Journal of Remote Sensing 2001;22:3813-3825.

[5] Prakash A, Gupta RP. Land-use Mapping and Change Detection in a Coal Mining Area-a Case Study in the Jharia Coalfield, India. International Journal of Remote Sensing 1998;19:391-410.

[6] Singh A. Digital Change Detection Techniques Using Remotely Sensed Data. International Journal of Remote Sensing 1989;10:989-1003.

[7] Jensen JR. Remote sensing of the environment -an earth resource perspective. Prentice-Hall, Inc., 2000.

[8] Salami AT, Ekanade O, Oyinloye RO. Detection of Forest Reserve Incursion In South-Western Nigeria From A Combination Of Multi-Date Aerial Photographs And High Resolution Satellite Imagery. International Journal of Remote Sensing 1999;20:1487-1497.

[9] Salami AT. Vegetation Dynamics on the Fringes of Lowland Tropical Rainforest Of South-Western Nigeria- An Assessment Of Environmental Change With Air Photos And Landsat. International Journal of Remote Sensing 1999;20:1169-1181.

[10] Petit CC, Lambin EF. Integration of Multi-Source Remote Sensing Data For Land Cover Change Detection. International Journal of Geographical Information Science 2001;15:785-803.

[11] Lu D, Mausel P, Brodizio E, Moran E. Change Detection Techniques. International Journal of Remote Sensing 2004;25**:**2365-2407.

[12] Zhou Q, Li B, Zhou C. Detecting and Modeling Dynamics Landuse Change Using Multitemporal And Multi-Sensor Imagery. In: ISPRS XXth Congress, Commission II, Working Group II/5, Istanbul, Turkey: 2004.

[13] Luque SS. Evaluating Temporal Changes Using Multi-Spectral Scanner and Thematic Mapper Data on the Landscape of a Natural Reserve: The New Jersey Pine Barrens, a Case Study. International Journal of Remote Sensing 2000;21:2589-2611.

[14] Alhameli S, Alshehhi M. Images Are An Outstanding Evidence Of Rapid Development "A Perfect Example From United Arab Emirates (UAE)". In: Proceedings of the ISPRS XXth Congress, Commission PS IC, Working Group II/4, XXXV, part B4. Istanbul, Turkey: 2004. p. 505-*ff*.

[15] Yagoub M M. Monitoring of Urban Growth of a Desert City Through Remote Sensing: Al-Ain, UAE, Between 1976 and 2000. International Journal of Remote Sensing 2004;25:1063-1076.

[16] Lo CP, Shipman RL. A GIS Approach To Land-Use Change Dynamics Detection. Photogrammetric Engineering and Remote Sensing 1990;56(11):1483-1491.

[17] Mouat DA, Lancaster J. Use of Remote Sensing and GIS to Identify Vegetation Change in the Upper San Pedro River Watershed, Arizona. Geocarto International 1996;11:55-67.

[18] Chen X. Using Remote Sensing and GIS to Analyze Land Cover Change and Its Impacts on Regional Sustainable Development. International Journal of Remote Sensing 2002;23:107-124.

[19] Weng Q. Land use Change Analysis in the Zhujiang Delta of China Using Satellite Remote Sensing, GIS and Stochastic Modeling. Journal of Environmental Management 2002;64:273-284.

[20] Terry S. Change Analysis in the United Arab Emirates: An investigation of techniques. Photogrammetric Engineering and Remote Sensing 1999;65(4):475-484.

[21] Liu H, Zhou Q. Accuracy Analysis of Remote Sensing Change Detection by Rule-Based Rationality Evaluation with Post-Classification Comparison. International Journal of Remote Sensing 2004;25(5):1037-1050.

[22] Michael J, Starbuck, Juanito T. Monitoring Vegetation Change in Abu Dhabi Emirate From 1996 To 2000 And 2004 Using Landsat Satellite Imagery. In: Second International Kuwait Conference. Kuwait: 2006. p. 817-831.

PERFORMANCE OF COMPRESSION IGNITION ENGINE WITH INDIGENOUS CASTOR OIL BIO DIESEL IN PAKISTAN

Mohammed Harun Chakrabarti[1], Mehmood Ali[2]

ABSTRACT

Castor oil available indigenously in Pakistan was converted successfully to bio diesel and blended to 10% quantity (by volume) with high speed mineral diesel (HSD) fuel. This fuel was tested in a compression-ignition engine in order to assess its environmental emissions as well as engine performance parameters. The blended fuel was found to give lower environmental emissions in most accounts except for higher CO_2 and higher NO_X. In addition, three engine performance parameters were assessed, which were engine brake power, engine torque and exhaust temperature. In the first two cases, blended bio diesel fuel gave lower figures than pure mineral diesel due to lower calorific value. However, its higher flash point resulted in higher engine exhaust temperatures than pure mineral diesel. Overall, in terms of engine performance, castor oil bio diesel (from non-edible oil of castor bean – growing on marginal lands of Pakistan) fared better in comparison to canola oil bio diesel (from expensive edible oil) and can be recommended for further tests at higher blend ratios.

Keywords: Castor, compression-ignition, bio diesel, indigenous, non-edible.

1. INTRODUCTION

Pakistan, being an energy deficient country tends to import foreign petroleum fuel in order to sustain. This has lead to loss of revenue in addition to the non-harnessing of indigenous resources to meet the energy demands of an ever growing population. Petroleum fuel is well known to be present in limited supplies throughout the world and have thus been classified as non-renewable sources of energy. These fuels also tend to produce harmful emission products of combustion that cause major damage to the ecological environment [1]. Such alarming impacts are easily visible within the urban environments of Karachi. As a result, a new alternative is being sought in order to try and circumvent the damage caused by harmful pollutants into the environment. In this respect, bio diesel has emerged as an ideal candidate for gradually replacing mineral diesel fuel in the near future. Bio diesel has shown tremendous environmental benefits as an alternative fuel [2-6] and has thus been considered to be implemented slowly and steadily in this country. The government of Pakistan has passed a recent law that by the year 2015, at least 5-10% of bio diesel must be blended with mineral diesel fuel for use in the diesel run automobile industry. Various organizations in Pakistan have begun work in this regard but the literature lacks relevant results from their endeavors.

[1] *Associate Professor, Department of Environmental Engineering, NED University of Engineering and Technology, Karachi – 75270, Pakistan. Ph. + 92-21-9261261-68 ext. 2225, Fax. + 92-21-9261255, Email: harun@neduet.edu.pk*

[2] *Assistant Professor, Department of Environmental Engineering, NED University of Engineering and Technology, Karachi – 75270, Pakistan. Ph. + 92-21-9261261-68 ext. 2271, Fax. + 92-21-9261255, Email: mehmood@neduet.edu.pk*

Manuscript received on 27th October 2008, reviewed and accepted on 14th April 2009 as per publication policies of the *NED University Journal of Research*. Pertinent discussion including authors' closure will be published in June 2010 issue of the Journal if the discussion in received by 30th November 2009.

Mohammed Harun is an Associate Professor and Co-Chairman in the Department of Environmental Engineering at the NED University of Engineering and Technology, Karachi, Pakistan. He received his Bachelors and Masters in Chemical Enginering and Chemical Technology from Imperial College London in 1999. He received his PhD in Chemical and Environmental Engineering from Manchester University UK in 2003. He has published several articles on bio diesel.

Mehmood Ali is an Assistant Professor in the Department of Environmental Engineering at the NED University of Engineering and Technology, Karachi, Pakistan where he received his BEngg and MEngg in Mechanical and Environmental Enginering, respectively, in 1995 and 2002. He has supervised two independent study projects of Masters students on bio diesel production.

However, it is known that their work have focused on oils from the Jatropha plant and the pongame plant, as has been done repeatedly in India since the past decade [7-10]. Due to this issue, work has begun in earnest in the Department of Environmental Engineering, NED University to try and produce some useful results for the literature regarding the possibility of producing bio diesel from indigenous vegetable oils to try and meet the target set by the government of Pakistan [11]. Canola oil from indigenous sources has been converted successfully to bio diesel [11] and has also been tested in a compression-ignition engine in a separate work [12]. Results obtained were found to be consistent with the literature [13]. However, canola is an edible oil and cannot be grown easily on marginal lands of Pakistan. Hence, other oil varieties bearing non-edible qualities have been investigated in the literature, such as jatropha, pongame and castor [7-10, 14-16]. In this work, it was decided to investigate the possibility of converting indigenous castor oil to bio diesel [17] and then having it evaluated in a compression-ignition engine as a potential resource for the benefit of Pakistan. This was because the native castor bean plant has a greater ability to grow on marginal lands than the other non-edible oil yielding plants mentioned above [17].

2. EXPERIMENTAL TESTING

2.1 Composition of Castor Oil

The basic composition of any vegetable oil is triglyceride, which is the ester of three fatty acids and one glycerol. The fatty acid composition of indigenous castor oil was determined using the procedures outlined in the literature [18].

2.2 Bio Diesel Production

A two step 'acid–base' process, acid-pretreatment followed by main base-transesterification reaction, using methanol as reagent and H_2SO_4 and KOH as catalysts for acid and base reactions, respectively, was followed to produce bio diesel from refined castor oil in a laboratory scale processor [11, 17]. Indigenous canola oil was converted to bio diesel as per the procedure outlined in the literature [11].

2.3 Fuel properties

A series of tests were performed to characterize the properties of the produced bio diesel. These properties include density (ASTM D 1298), kinematic viscosity (ASTM D 445), cetane index (ASTM D 976, EN ISO 4264), flash point (ASTM D 93) as well as water and sediment contents (ASTM D 2709).

2.4 Engine emissions

The specifications of the compression-ignition engine (CIE) used in this work is described in **Table 1**. The fuel tested in the engine consisted of 100% High Speed Diesel (HSD) and 10% bio diesel with 90% diesel (B10), respectively. Emissions analysis from the diesel engine specified in **Table 1** was conducted at a constant speed of 2,600 rpm. The emission measurement system consisted of a self calibration exhaust gas analyzer (Testo Instruments Ltd.) and measurements were carried out in a similar manner to those of other workers [5]. The analyzer consisted of a number of probes including a temperature monitor. Parameters measured by means of the gas analyzer included carbon dioxide (CO_2), carbon monoxide (CO), oxides of nitrogen (NO_X), sulphur dioxide (SO_2) and particulate matter (PM). The engine was operated at 100% throttle and particulate matter was analyzed by means of a hand held device collecting exhaust particles on filter papers.

Table 1. Engine specification

Make	Rotronics
No. of Cylinders	2
Maximum Speed	2700 rpm (283 rad/s)
Bore	72 mm (2.83 in.)
Stroke	62 mm (2.44 in.)
Type	Four stroke, direct injection, air cooled
Injector opening pressure	12753 kPa (1849.2 lb/in$^{2)}$
Displacement volume	505 cm^3 (30.82 in^3)
Oil Quantity	1.6 liters (0.057 ft^3)
Dry Weight	60 kg (132.3 lb)
Compression Ratio	8.5:1
Maximum output	2.0 kW (2.68 hp)
Nominal power	1.8 kW (2.41 hp)
Volume of cylinders	380 c.c. (23.2 in^3)

2.5 Engine performance

Engine performance was measured using 100% HSD and B10 only. This blend ratio was in line with the target imposed by the Government of Pakistan to blend up to 10% bio diesel with mineral diesel for the automobile sector by the year 2015. The performance of the engine was studied at different engine speeds following the procedures of other workers [6]. After the engine reached the stabilized working condition, gross brake power, engine torque applied and exhaust temperature were measured and analyzed [6].

3. RESULTS AND DISCUSSION

3.1 Fatty acid profile of castor oil

The fatty acid composition of indigenous castor oil was determined by means of gas chromatography as described in detail in the literature [17]. Results are reported in **Table 2**. The results obtained were very much consistent with those reported by other research workers [14, 15].

3.2 Fuel properties

The various fuel properties of castor oil, castor bio diesel (B100) and 100% high speed mineral diesel (HSD) as determined following the ASTM standards and procedures are summarized in **Table 3**. It can be seen from this table that the fuel properties of B100 are comparable with those of HSD and except for water content are well within the ASTM D 6751-02 and EN 14214 standards

Table 2. Fatty acid profile of castor oil

Fatty Acid	Values (wt. %)
Ricinoleic	90.2
Linoleic	4.4
Oleic	2.8
Estearic	0.9
Palmitic	0.7
Dihidroxiestearic	0.5
Licosanoic	0.3
Linolenic	0.2

Table 3. Fuel properties of castor oil, castor oil bio diesel and HSD

Parameters	High speed Diesel (HSD)	Castor Oil	Castor B100	Test Method
Density at 20 °C g/cm^3 (lb/in^3)	0.83 (0.027)	0.9584 (0.032)	0.9245 (0.031)	ASTM D 1298
Kinematic Viscosity mm^2/s (in^2/s)	2.73 (0.0042)	239.39 (0.371)	13.75 (0.0213)	ASTM D 445
Cetane Index	46	43	50	ASTM D 976
Flash Point °C (K)	37 (310)	310 (583)	120 (393)	ASTM D 93
Water and sediment vol. %	< 1	Nil	0.05	ASTM D 2709

for bio diesel [14, 17]. The castor oil and its bio diesel, however, was found to have much higher values of fuel properties, especially viscosity, way above any of these standard limits – thus restricting its direct use as a fuel for diesel engines. Similar conclusions were also discovered by other research workers [17].

3.3 Engine emissions

The high viscosity of the castor bio diesel limited maximum blend ratio to 10% only by volume (B10). The emissions of CO_2, CO, NO_X, and SO_2 against fuel type are shown in **Figs. 1 to 4**, With exception to the increases in carbon dioxide and oxides of nitrogen emissions with more bio diesel blended in the fuel mixtures, all other pollution parameters were found to decrease in general. Results were similar to those reported by other research workers [19]. In diesel engines without exhaust gas recirculation (EGR), the combustion of bio diesel almost always results in higher CO_2 in exhaust gases in comparison to diesel fuel combustion irregardless of fuel injection type used (**Fig. 1**). This is due to the presence of more carbon atoms as well as higher oxygen content in bio diesel fuel. In addition, bio diesel is more fuel-rich than diesel fuel thus resulting in higher combustion temperatures and high exhaust gas temperatures (**Fig. 5**). These reasons result in less oxygen content in exhaust gases obtained from the combustion of bio diesel fuel in comparison to mineral diesel fuel (**Fig. 6**).

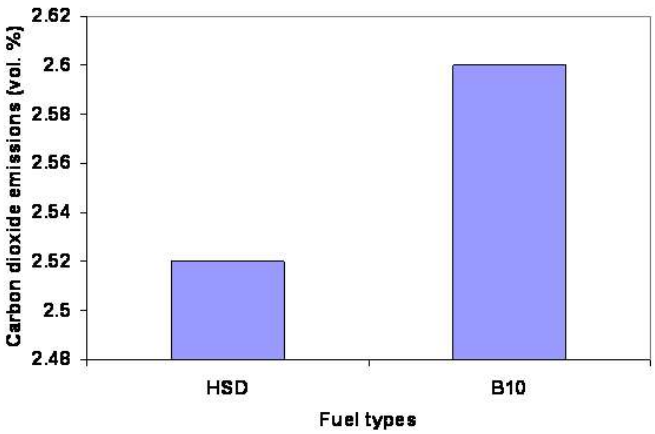

Figure 1. Carbon dioxide emissions from diesel engine operating on diesel fuel and castor B10.

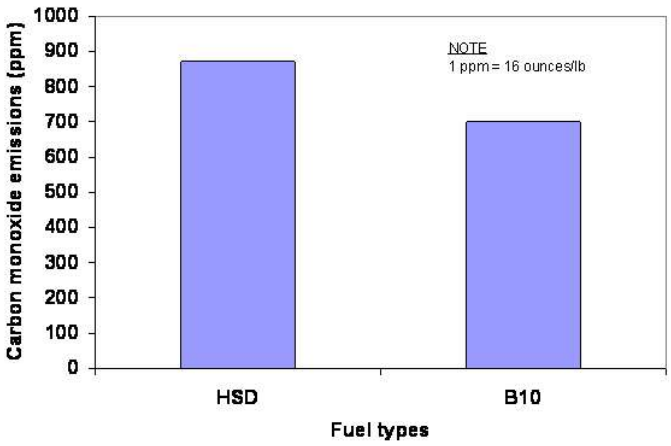

Figure 2. Carbon monoxide emissions from diesel engine operating on diesel fuel and castor B10.

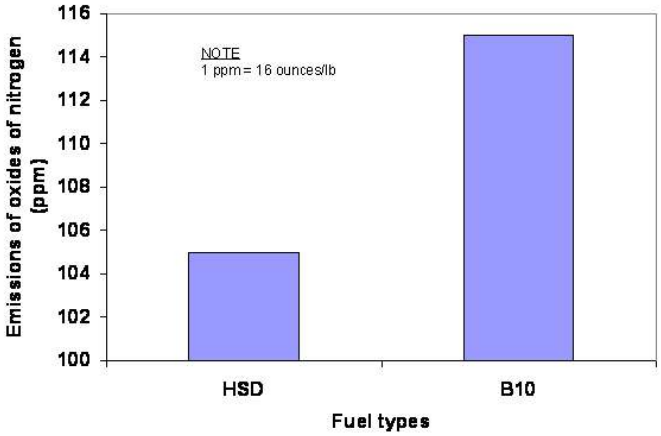

Figure 3. Emissions of Oxides of nitrogen from diesel engine operating on diesel fuel and castor B10.

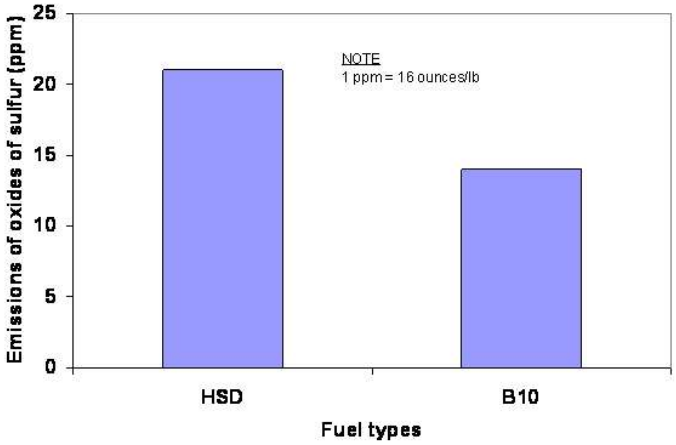

Figure 4. Emissions of sulphur dioxide from diesel engine operating on diesel fuel and castor B10.

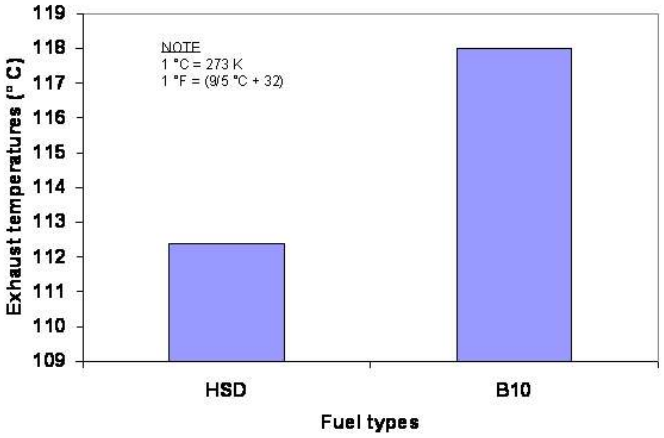

Figure 5. Exhaust temperatures of flue gases released by diesel engine operating on diesel fuel and castor B10.

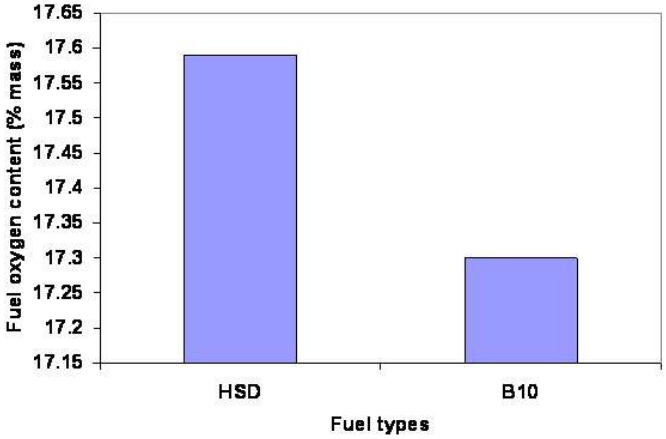

Figure 6. Fuel oxygen content in exhaust gases for diesel engine operating on diesel fuel and castor B10.

Particulate matter emissions from mineral diesel and blended bio diesel were also monitored. The results are displayed in **Fig. 7**. Particulate matter was found to decrease as expected when using castor B10 as engine fuel in comparison to mineral diesel fuel. Most of the results obtained are in full consistency with previous reported work conducted by other research workers [19].

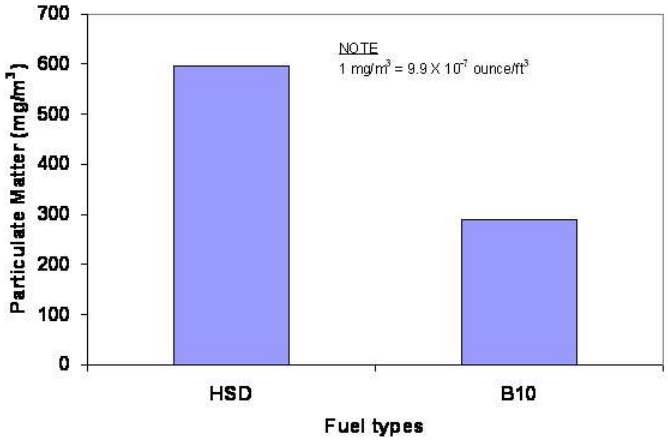

Figure 7. Particulate matter emissions from combustion of mineral diesel and blended bio diesel fuel in the compression ignition engine.

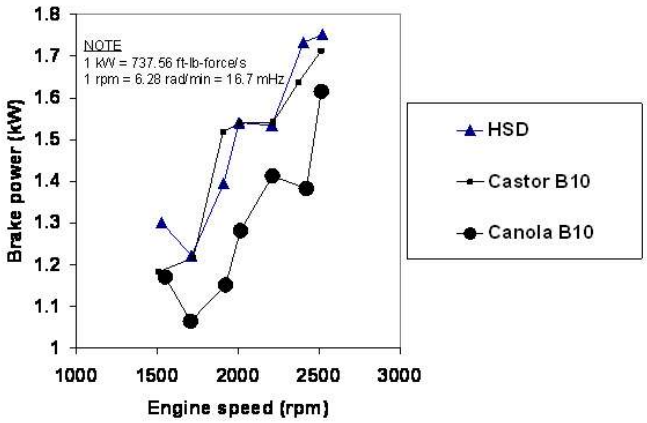

Figure 8. Variation of Engine Power against a range of engine speeds using three different fuel types (HSD; castor B10; and canola B10).

3.4 Engine performance

The engine performance of blends of castor oil bio diesel and mineral diesel (castor B10) was evaluated in terms of engine torque, engine exhaust temperature and engine brake power at different engine speeds of operation. Engine performance results of blends of canola oil bio diesel with high speed mineral diesel (canola B10) have been provided in this section for comparison purposes.

3.4.1 Brake Power

The variation of brake power for different engine speeds is highlighted in **Fig. 8**. Three different fuel types are depicted: HSD, castor B10 and canola B10. **Fig. 8** shows that there is slightly less power generated from blended bio diesel fuel as compared to mineral diesel fuel due to lower calorific value [11]. In addition, it was observed that blended castor bio diesel gave better engine power than blended canola bio diesel. The main reason for this is that the calorific value of castor bio diesel (38.7 MJ/kg) is higher than that of canola bio diesel (36 MJ/kg) [11].

3.4.2 Engine Torque

The variation of engine torque for different engine speeds is shown in **Fig. 9**. Three different fuel types are depicted: HSD, castor B10 and canola B10. The curves developed between mineral diesel and blended bio diesel showed that the petroleum diesel presented higher torque during engine testing. The reason for this was due to greater calorific value of mineral fuel in comparison to the bio diesel fuel. The graph pattern shows that initially more torque was required for operating the engine, but a gradual decline was observed with the passage of time (for all fuel types tested). Despite lower torque obtained, bio diesel still has some potential for employment in the compression-ignition engine and its performance can be improved as further research continues in this field.

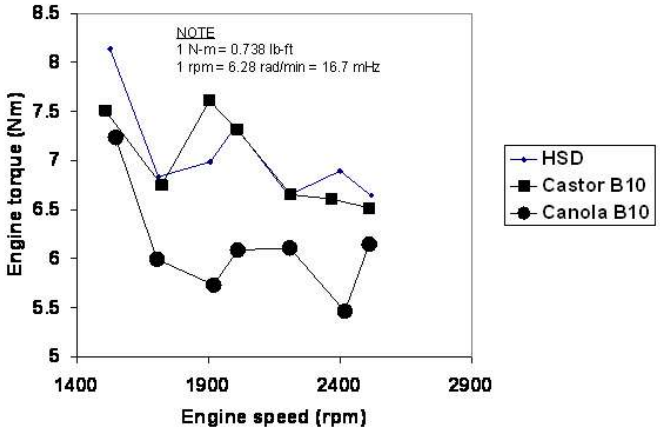

Figure 9. Variation of Engine Torque against a range of engine speeds using three different fuel types (HSD; castor B10; and canola B10).

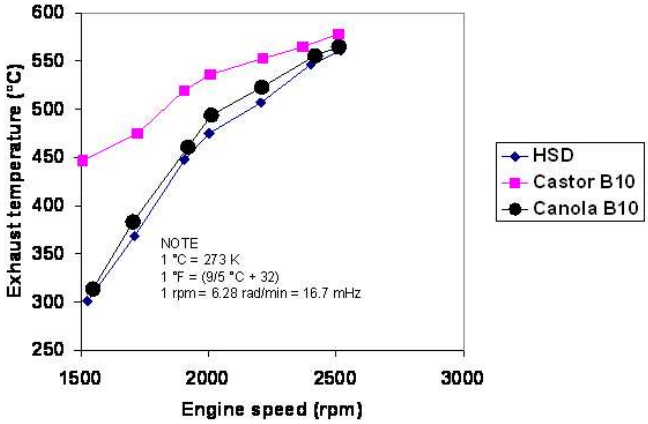

Figure 10. Engine Exhaust Temperatures against a range of engine speeds using three different fuel types (HSD; castor B10; and canola B10).

3.4.3 Engine exhaust temperature

Variation of exhaust gas temperatures against different engine speeds is illustrated in **Fig. 10**. Three different fuel types are depicted: HSD, castor B10 and canola B10. The exhaust gas temperature measurements showed that for mineral diesel fuel the temperature is less as compared to bio diesel blended fuel mixtures. This is basically due to a lower burning temperature developed in the combustion chamber when using mineral diesel as fuel. The burning of blended castor bio diesel was found to have the highest exhaust temperature as compared to blended canola bio diesel, due to its higher heating value and higher flash point [11, 17].

Bio diesel, having a higher oxygen content (as well as higher flash point) tends to burn at higher temperatures than mineral diesel fuel. In addition, the amount of injected fuel increases with the engine speed in order to maintain torque and power output [21]. Hence, the heat release rate and the exhaust temperatures from burning bio diesel rise with the increase in engine speed. One possible drawback of this is higher NO_X emissions, which may possibly be reduced by employing exhaust gas recirculation (EGR) technology as described in the literature [7].

4. CONCLUSIONS

Following conclusions may be drawn from the study reported in this paper.

1. Bio Diesel gives far less emissions than mineral diesel, except for carbon dioxide and NO_X. Higher CO_2 is released due to higher oxygen and carbon contents of bio diesel, thus signifying complete combustion of the fuel in compression-ignition engines. Higher NO_X releases are due to higher temperatures of combustion than mineral diesel fuel, but this could be reduced by employing catalytic converters or EGR.
2. The brake power and engine torque obtained with blended bio diesel fuel is less than that for mineral diesel fuel. This is mainly because of a lower calorific value of bio diesel in comparison to diesel.
3. Castor oil B10 gave higher brake power and engine torque in comparison to canola oil B10 (blended at 10% by volume).
4. Engine exhaust temperatures of blended bio diesel fuel mixtures are higher than that of pure mineral diesel, mainly due to the oxygenated nature of bio diesel.
5. Castor oil B10 gave higher exhaust temperatures than canola oil B10.
   Overall, castor oil bio diesel was found to give a better engine performance than canola oil bio diesel. This result is very positive because castor oil is not only non-edible but the castor bean plant can easily grow on marginal lands, thus making it a very valuable raw material for bio diesel production in Pakistan. However, before the castor oil can be recommended further, more work is necessary in trying to reduce its viscosity so that its bio diesel could meet the ASTM D 6751 standard limit [17]. If this could be achieved, higher blend ratios could be investigated in further work.

ACKNOWLEDGMENTS

The authors wish to acknowledge the financial support provided for this research by the Advanced Studies and Research Board (AS&RB) of the NED University of Engineering and Technology. The Department of Automotive and Marine Engineering, NED University is also acknowledged for testing different blends of bio diesel with mineral diesel in a compression-ignition engine. PCSIR Laboratories Karachi is gratefully acknowledged for helping with engine emissions testing using blended castor oil bio diesel fuel.

REFERENCES

[1] Cassedy ES and Grossman PZ. Introduction to Energy – Resources, Technology and, Society. England: Cambridge University Press, England, 1998. p. 135-147.

[2] Harun M, Ali M, Mustafa I. Environmentally Friendly Diesel for Pakistan. Environ Monitor 2006;6:14-18.

[3] Demirbas A. Biodiesel Impacts on Compression Ignition Engine (CIE): Analysis of Air Pollution Issues Relating to Exhaust Emissions. Energy Sources 2005;27(6):549-558.

[4] Korres DM, Karonis D, Lois E, Linck MB, Gupta AK. Aviation fuel JP-5 and biodiesel on a diesel engine. Fuel 2008;87(1):70-78.

[5] Lin Y, Wu YG, Chang CT. Combustion characteristics of waste-oil produced biodiesel/diesel fuel blends. Fuel 2007;86:1772-1780.

[6] Raheman H, Ghadge SV. Performance of compression ignition engine with mahua (Madhuca indica) biodiesel. Fuel 2007;86(16):2568-2573.

[7] Pradeep V, Sharma RP. Use of HOT EGR for NOx control in a compression ignition engine fuelled with bio-diesel from Jatropha oil. Renewable Energy 2007; 32(7):1136-1154.

[8] Reddy JN, Ramesh A. Parametric studies for improving the performance of a Jatropha oil-fuelled compression ignition engine. Renewable Energy 2006; 31(12):1994-2016.

[9] Modi MK, Reddy JRC, Rao BVSK, Prasad RBN. Lipase-mediated transformation of vegetable oils into biodiesel using propan-2-ol as acyl acceptor. Biotech Let 2006;28:637-640.

[10] Rathore V, Madras G. Synthesis of biodiesel from edible and non-edible oils in supercritical alcohols and enzymatic synthesis in supercritical carbon dioxide. Fuel 2007;86:2650-2659.

[11] Chakrabarti MH, Ali M. Bio Diesel from Refined Canola oil in Pakistan. NED University J Res 2008;5(1):34-42.

[12] Chakrabarti MH, Ali M. Engine Emissions Testing of Indigenous Bio Diesel / Diesel Fuel Blends in Pakistan. NED University J Res 2008;5(2): 1-9.

[13] Nwafor OMI. Emission Characteristics of Diesel Engine Operating on Rapeseed Methyl Ester. Renew Energy 2004;29(1):119-129.

[14] Conceicao MM, Candeia RA, Silva FC, Bezerra AF, Fernandes Jr. VJ, Souza AG. Thermoanalytical characterization of castor oil biodiesel. Renew Sustain Energ Rev 2007;11:964-975.

[15] Conceicao MM, Fernandes Jr. VJ, Bezerra AF, Silva MCD, Santos IMG, Silva FC, Souza AG. Dynamic Kinetic Calculations of Castor Oil Biodiesel. J Thermal Anal Cal 2007;87(3):865-869.

[16] Silva NDLD, Maciel MRW, Batistella CB, Filho RM. Optimization of Biodiesel Production From Castor Oil. Appl Biochem Biotech 2006;129-132:405-414.

[17] Chakrabarti MH, Ahmad R. Transterification studies on castor oil as a first step towards its use in Bio Diesel production. Pak J Bot 2008;40(3):1153-1157.

[18] Bhatti HN, Hanif MA, Qasim M, Rehman A. Biodiesel production from waste tallow. Fuel 2008;87:2961-2966.

[19] Lapuerta M, Armas O, Rodriguez-Fernandez J. Effect of biodiesel fuels on diesel engine emissions. Prog Energy Comb Sci 2008;34(2):198-223.

[20] Forero CLB. Bio diesel from castor oil: a promising fuel for a cold weather, 2005 (accessed on 25 October 2008). Available from http://www.icrepq.com/full-paper-icrep/222-barajas.pdf

[21] Lin CY, Lin HA. Diesel engine performance and emission characteristics of biodiesel produced by the peroxidation process. Fuel 2006;85(3):298-305.

HOUSEHOLD ACCESSIBILITY ANALYSIS IN DEVELOPING COUNTRIES USING TIME-SPACE PRISM

Mir Shabbar Ali[1]

ABSTRACT

Time geography approach provides quantifiable measures in the form of Time-space prisms which are used for analyzing individual activity spaces resulting from household activity-travel decisions. In the recent concerns to improve accessibility of rural households in developing countries, the need to develop a framework to study economics of household decision-making in the light of their time-space constraints has become profound. This paper presents a conceptual framework based on time geography approach which was used to study constraints limiting accessibility of work places. Data collected from rural locations in Pakistan was used to demonstrate how the economics of household decision-making formulates their accessibility to various activities duly transformed by the available transportation system, which includes both the vehicles as well as the network.

Keywords: Activity-travel patterns, developing countries, household economics, household decision-making, time geography, time-space prism

1. INTRODUCTION

Study of time budget constraints is a key to quantify economic deprivation of populations of developing countries. Time geography approach integrates time and space dimensions in order to study autonomy of an individual and is able to investigate individual activity-travel behaviour under constraints, [1]. Time is viewed both to overcome the spatial separation of activities as well as the constraints on the individual. Measures based on this approach conceive the activity programme of an individual in terms of probability of activity participation. This is closer to the definition of accessibility that concerns the opportunity an individual, placed at a given location, possesses in order to take part in activities [2].

Time-space paradigm is able to provide framework for analysis of activities 'accessible' to individuals under the economics of household decision-making. The objectives of this paper include (i) to explain the embedded concepts of time-space prism as a means to quantify accessibility measures and (ii) to demonstrate their applications in studying individual activity-travel patterns under household economic constraints.

[1] *Professor, Department of Urban and Infrastructure Engineering, NED University of Engineering and Technology, Karachi, Pakistan, Ph. +92 (021) 9261261,Ext 2354, Fax. +92 (021) 9261255, Email mshabbar@neduet.edu.pk*

Manuscript received on 29th September 2008, reviewed and accepted on 02nd May 2009 as per publication policies of the *NED University Journal of Research*. Pertinent discussion including authors' closure will be published in June 2010 issue of the Journal if the discussion is received by 30th November 2009.

Mir Shabbar Ali is a Professor and Chairman in the Department of Urban and Infrastructure Engineering at NED University of Engineering and Technology, Karachi, Pakistan, where he received his BEng in Civil Engineering in 1983. He received his MEng in Structural Engineering from University of Oklahoma, USA and PhD in Transportation Engineering from the University of Birmingham in 1987 and 2001, respectively. His research interests include transportation planning, travel demand modelling and geometric and pavement design.

2. TIME-SPACE PRISM

The 'time-space prism' (TSP) of an individual considers time as a fixed constraint on the individual and 'delineates' the sequence of activities 'possible' during a time period (say a day). Two important elements of time used are (i) the minimum time required by the activity and (ii) the maximum time to be spent travelling. The TSP of a hypothetical rural individual is illustrated in **Figure 1**. The individual is free to move in all directions at a uniform speed v1. The horizontal axis represents space in linear dimensions (for example projected distances) and the vertical axis represents time. This simplified prism gives the total time budget available to the individual (e.g., between 8 a.m. and 1 p.m.). This general prism is then constrained on the basis of some further coupling constraints on the individual (i.e. to be present at certain places at certain times). An example is given below to define the basic concepts and terminology used [3].

Consider a school-going child selected from a hypothetical rural household. In **Figure 1** '2-D map' is shown along with time-space prism of this individual. A primary school at location A, having less facilities, is reachable in one hour. Another primary school, at location B, having a higher quality of education, is at a further hour's journey from location A. Both schools have the same 'opening hours' (9AM-4PM). The time-space prism of the child enables a transportation planner to assess the child's ability to reach to location A at 9AM and his inability to reach location B by 9AM. Thus the child's transport, temporal and spatial constraints define his capability to reach any of these activities. In other words, his TSP is able to define the accessibility of the activity, namely "attending school".

Time-space prism maps out the individual opportunities under effect of time-space constraints governing activity travel patterns of individuals in a developing as well as developed country context [4]. Significant differences have been reported to exist between workers and non-workers and between males and females, due to the more traditional gender and working status roles in a developing country context. The approach, therefore is able to address cultural constraints binding heavily on individuals in a developing country [5,6].

Description of salient points in TSP:
ac=Total time budget
ef,gh, ij = activity duration at locations A, B and Q, respectively
ae, ai, ag = travel from home to activity locations A, B and Q, respectively
fc, jc, hc = travel to home from activity locations A, B and Q, respectively

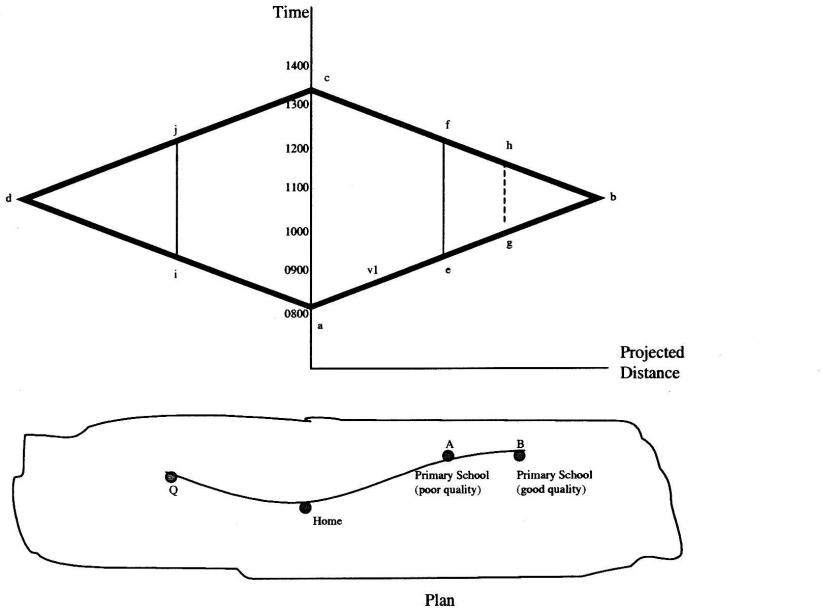

Figure 1. Time-Space autonomy of individuals

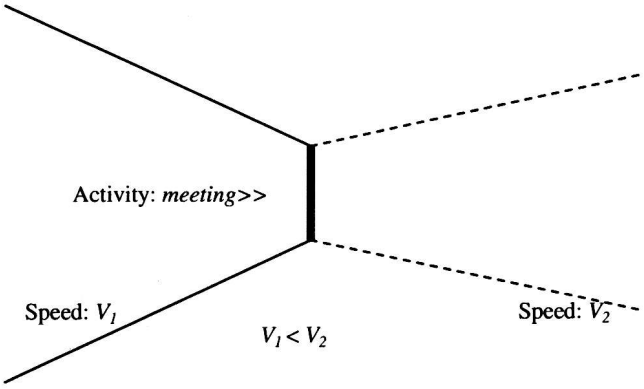

Figure 2. Explanation of coupling constraints

2.1 Accessibility Measures based on Time Geography Approach

Time geography measures view the activity programme of an individual in terms of taking part in activities. Burns [7] developed an analytical formulation to incorporate all the components of accessibility, the transportation, temporal and spatial components, in a single framework. He added temporal dimensions to the conventional 'spatial-accessibility' approach, which treated the ability of individual to reach the activities independent of his time constraints, both on the activity and the individual. The underlying assumption is that individuals value opportunities available to them in relation to the time budget at their disposal. He defined an opportunity through three non-negative numbers; the distance to travel (x), the attributes of the opportunity (a) and the duration of time (T). Burns [7] represented an opportunity by means of an ordered triad (x,a,T). The accessibility benefit measure developed by Burns [7] was improved by Odoki [8,9] and adapted for application for rural accessibility planning in developing countries [10]. The salient features of his model have been:

a) The transport component is weighted by a generalised cost function, which not only incorporates the deterrent effect of travel on the individual's perception of the utility of opportunity, but also weighted on the basis of his income,
b) The household perception is added as a factor in weighting the attributes of the spatially separated activities typical of rural areas of developing countries,
c) Contrary to the population weighted opportunities, this approach caters for value weighted opportunities conforming to the individual's space-time autonomy.

Jones, et al. [11] provided a framework whereby travel is traced in two dimensions, i.e. space and time; as a result sequencing becomes the key element of activities, hence trips. Ben-Akiva [12] indicated a change in perspective on the travel demand modelling approach, from purely a transportation system oriented approach to the activity-behaviour approach. The basic theme is that the demand for travel is derived from demand for activities. Wu et al [13] explored dynamics of time-space prism and developed network-based TSP's. They applied these concepts to evaluate accessibility of travellers under different congestion scenarios, alternative network flow control strategies, and activity scheduling policies. An example of coupling constraints is given in **Figure 2** which depicts the need of two individuals to be at one place (for example for a meeting) while both arrive there at their own pace (v1 and v2).

All the above studies put stress on analysis of individual activity-travel pattern while prime concern is on time-budget constraints and to devise measures for alleviating these constraints. The following sections of the paper deliberate this task further on.

2.2 Time-space distribution of activities and travel

Participation in the spatially distributed activities defines travel pattern of an individual in a given period of time. The activities which can be 'placed' within the TSP of an individual are termed as opportunities [9]. The sequence of this activity participation is studied in a two-dimensional time-space plane which provides insight of the individual time budget constraints. It therefore helps in devising planning strategies relieving these constraints.

Time-space prism of **Figure 3**, shows the activity-travel sequence of an individual starting and ending at times A & B, respectively. The inclined lines show the instantaneous positions of the time-space prism available to the individual after he decides to participate in any activity (the vertical

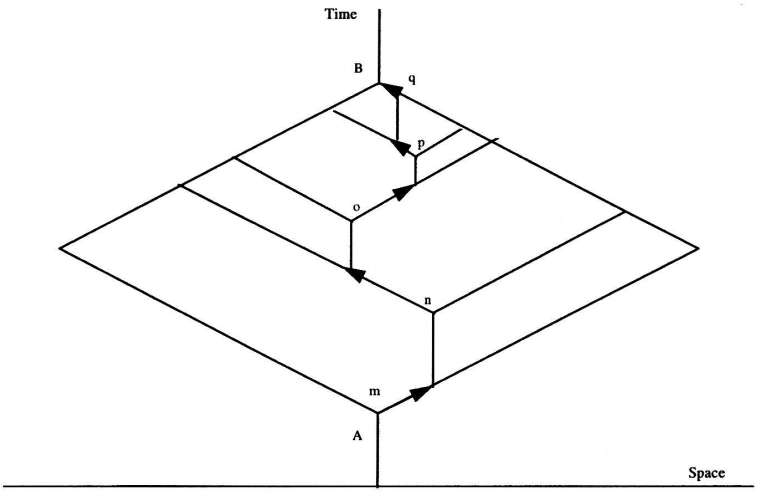

Figure 3. Time-space distribution of activities and travel

lines). The arrows show trips at the maximum uniform velocity. It is clear that the activity-space is rearranged after the individual participates in an activity. Four 'successive' positions of the activity space are generated in the figure as a result of three activities. The travel between activities defines trips; their sum defines total trips of the individual in one day.

Time-space prisms are used in analysis of activity-travel pattern of individuals and temporal vertices of time-space prisms are compared for various socio-economic and commute characteristics [14]. Kwan [15] suggested that modern spatial analysis tools embedded in a GIS environment would enable comprehensive representation of complex urban and cognitive environments more realistically by overcoming limitations of aggregate spatial data framework. Miller and Wu [16] argued that space-time accessibility measures (STAMs) reflect the benefits that individuals receive from the transportation system. They are easily interpreted, particularly with respect to changes in accessibility. This is critical as (in their opinion) transportation systems exist to improve individual accessibility.

3. RELEVANVE TO RURAL ACTIVITY-TRAVEL PATTERNS IN DEVELOPING COUNTRIES

The rural travel pattern in developing countries is dominated by travel required to access basic needs and services [17]. It has been reported that the time spent on such travel is relatively constant throughout the year [18]. Rural individuals (especially women and children) spend approximately 0.3-1.5 hours daily in acquiring basic needs like water and firewood. Poor access is also responsible for critical problems like high mortality rates, inadequate food security, and improper education [17]. It is therefore important to understand this issue in order to ascertain productivity of new infrastructure investments.

A common conclusion of a number of studies is that the wastage of time in acquiring access to basic needs and services is responsible for non-achievement of development objectives [18, 19]. These studies also emphasize that transport should be considered in its facilitating role of providing access at household level, [18]. Bryceson and Howe [19] strongly suggested the need to understand women transport logistics relating agricultural needs, household essential services and childcare, in multitasking (all in one) trip strategies.

Ellis [20] studied the mobility aspects of rural accessibility. He analyzed the effects of the provision of transport services for a given infrastructure in reducing operating costs and enhancing mobility. Howe [21] found that non-availability of low-cost transport modes was a major source of decreased mobility and increased poverty of rural population in Sub Saharan Africa. Both these works addressed personal mobility as an important determinant of rural accessibility in least developed countries.

It is important to recognize that a major part of rural travel in developing countries comprises of access to activities or services fulfilling basic needs. These needs are emanated at the household level where individual members are assigned specific roles of activity participation. The distribution of responsibilities of individuals carrying out these activities is very much dependant on the cultural binding rather than on an equal sharing of the workload. For example, in rural areas of Pakistan, women do not go out for shopping daily consumables, simply because of cultural constraints.

Therefore the male members of the household have to schedule these activities into their time frame. The household role allocation is an important consideration in defining the purpose and frequency of rural personal travel.

The current focus is on the link between accessibility and rural development in developing countries. This requires an understanding of travel patterns within the framework of accessibility of activities. The proposed framework should enhance existing rural transportation planning methodologies. In rural areas of Pakistan, the major household activity-travel distribution is such that the main burden of 'travel-related-economic' activities (for example work, shopping for essentials) rests on adult male members while the main 'non-travel' activities (for example household chores) as well as some specific 'daily need' activities (water and firewood collection) rest on the adult female members [3]. In the above backdrop a study area was selected from rural settlements of Pakistan such that villages were selected from five clusters of varying distance from major market centre [3]. Details are presented in sections to follow.

4. HOUSEHOLD ACTIVITY-TRAVEL PATTERN ANALYSIS

Household level data was collected from selected two rural locations in Pakistan [3]. These rural areas belonged to Hala, Sindh, a province situated in the south-most part of Pakistan. Its rural areas are predominantly agricultural based. The experiment design was based on the premise that individual activity-travel pattern is a result of the role of the individual within the household. It assumes that household needs are transformed into activities performed by household individuals. A variable called Life Cycle Stage (LCS) was introduced to capture household role allocation dynamics, (**Figure 4**).

4.1 Experiment design and sampling

The cluster method of design was adopted in this research to address spatial dispersion of population more effectively. The area set up is such that a district level administration is the centre of all major activities (for example market, high schools, etc) and fulfils the requirements of several villages in the adjoining areas, under its administrative control. Moreover, these villages being culturally and geographically homogeneous units, serve an adequate setting to be considered as clusters. In survey design five clusters were formed on the basis of distance from the market centre. From each cluster one village was sampled at random to constitute the first level stratum. The sampling of twenty households within the selected village was also done on a random selection basis. **Table-1** summarises the general characteristics of villages where household surveys were carried out.

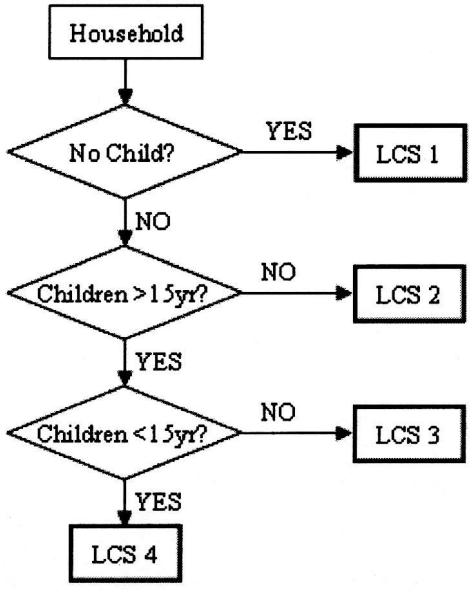

Figure 4. Life Cycle Stages Concept

Table 1. Sampled population

Cluster	Village	No.of Households	No.of Individuals	Male	Female	Indiv. Per HH
1	Hala Old	20	93	52	41	4.7
2	Khandu	20	69	34	35	3.5
3	Saeed Khan Leghari	20	94	55	39	4.7
4	Mansoora	20	70	40	30	3.5
5	Wngheri	20	47	23	24	2.4
		100	373	204	169	3.7

Table 2. Legends used in activity diary

Travel	Non Home Activities	Home-based Activities
0 Walk	9 Work/school	16 Home
1 Animal cart	10 Shop	17 Handicraft/ business
2 Bicycle	11 Hospital	18 House-chores
3 Tractor trailer	12 Leisure	
4 Motor cycle	13 Firewood collection	
5 Private car / jeep	14 Water collection	
6 Hired car/jeep	15 Other	
7 Bus		
8 Other		

4.2 Daily activity analysis

It is worth mentioning that in this research the Work was defined as the primary earning-related activity for any household individual. The following earning-related categories were used to define activity Work (as a part of detailed field survey):

(1) Waged Agricultural Labour
(2) Own Farm Agricultural Labour
(3) Waged Non- Agricultural Labour
    a) Office / indoor work
    b) Outdoor / field work
(4) Self Employed Non- Agricultural works
    a) Office / indoor work
    b) Outdoor / field work
(5) Other (specify)

The individual activity-travel patterns, therefore, provide information regarding the household role allocation and subsequently the fulfilment of household needs. The activity-travel pattern of an individual is, therefore, a function of (a) the individual category (for example Head, Wife, Child etc.) and (b) the activity type (for example Work, Shopping, School, etc.)

Individual activity-diaries were processed to divide total daily time (0600 to 2100) into 15-minute time slots (64 in total). All of these slots were non-blank and contained one number, between 0 and 18, on the basis of information derived from individual's activity diary. The description of the legends for these numbers is given in **Table 2**.

The legends given in **Table 2** were used to place each individual in one of the three states, namely, Travelling (0-8); Non-home activities (9-15); Home-based activities (16-18) **Figure 5** illustrates the daily activity-travel pattern of the Household Head. The percentage of the sample, within the individual category, carrying out a certain activity (or travel) at each time slot for the whole day (0600 to 2100) is plotted against the time.

The graphs in **Figure 5** provide the aggregate distribution of the population in the three states (home-based activities, non-home activities, or travel) at a given time. Most of the household heads leave home around 8:00am. The return journeys are spread between 13:00 to 21:00. The presence of these individuals at home is almost negligible within the working hours, i.e. 09:00 to 13:00. A peak for return journeys was formed around 14:30.

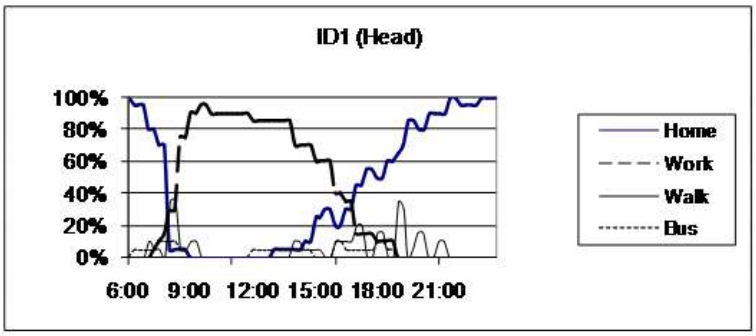

Figure 5. Daily activity travel pattern of household head

4.3 Cultural and gender effects

Similar analysis was performed for all household individuals. For the purpose of this analysis, individuals named “child>15 years” and “child<15 years” were further divided into male and female categories to highlight the discreteness in their activity-travel patterns. **Figures 5-7** show the activity-travel pattern of male and female individuals (respectively). Each of the individual category exhibits a discrete activity-travel pattern.

In general the graphs provide insight into overall time-budget of various individual categories. The state of home-based activities approaches 100% near the two ends of the day (around 0600 and 2000), when most of the individuals are at home. In the mid-day period most individual are at 'non-home' locations, (except for a few individual categories). The maximum percentage travelling was around 60%, (even in the case of the household head), explaining the role of travel in accessing daily activities.

On the aggregate basis, the household heads have involvement in 'non-home' activities for a longer part of the day, in comparison to any other individual category. The activity-travel pattern of the household wife and the female child (>15 years) were found to be similar. This explains the cultural effects on access to activities. A small percentage of housewives have been involved in travelling. The probable reason is for carrying out household chores like water collection, etc.

It is worth mentioning here that **Figures 5 - 6** only contain either of the two non-home activities, i.e. Work or School. At any particular instance of time, therefore, the total of the vertical axis may not sum to 100%. This indicates involvement of individual category in activities other than Work or School.

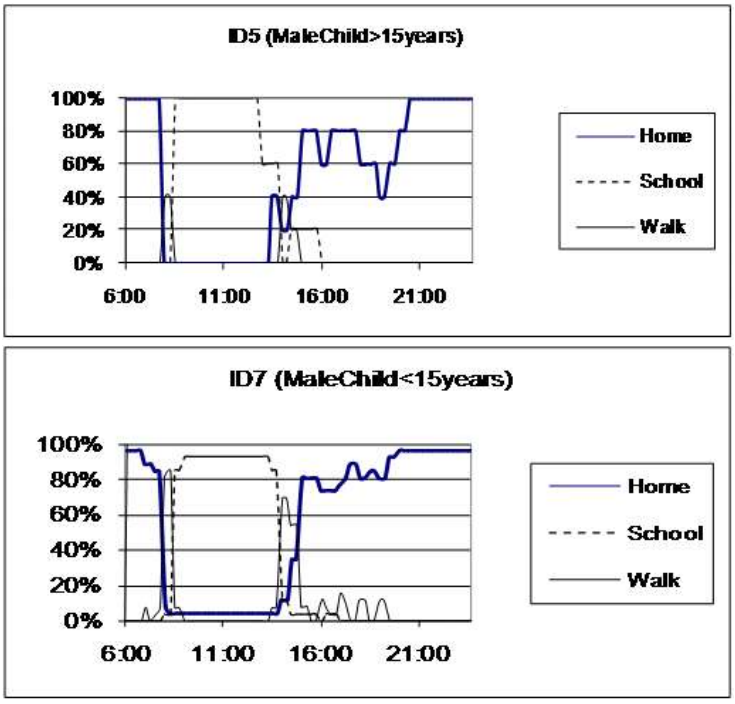

Figure 6. Daily activity-travel pattern by male individuals (all types)

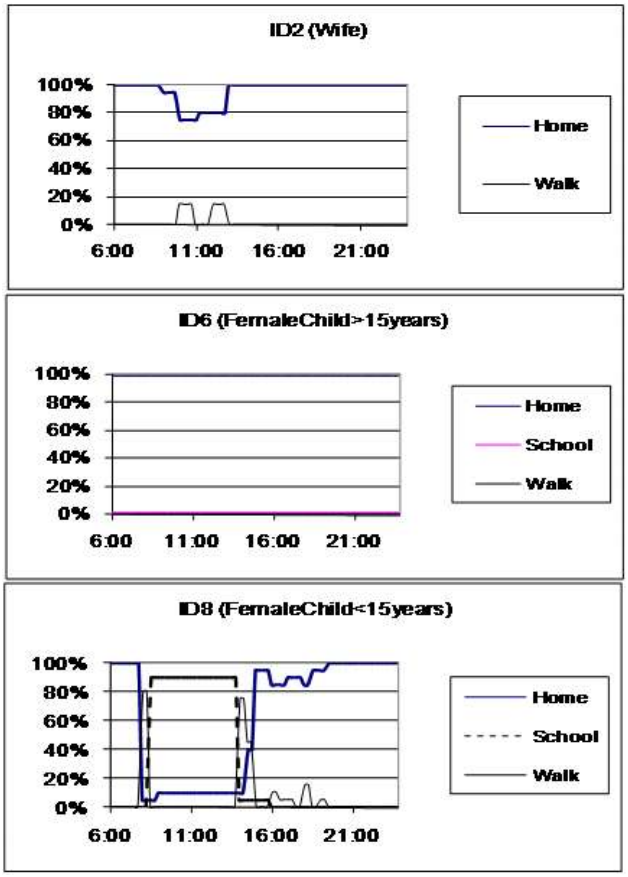

Figure 7. Daily activity-travel pattern by female individuals (all types)

4.4 Economics of household decision-making

The economics of rural household decision-making is derived on the basis of their involvement in earning-related activities. In a typical developing country context, Household Heads are the main individuals responsible for carrying out Work activities [3,5]. **Figures 5 - 7** support the derivation. This has become the basis of analyzing in detail the accessibility characteristics of household heads as presented in the sections to follow.

4.5 Vehicle ownership and time-space prisms

The transportation, temporal and spatial constraints binding upon individuals define their time-space prism (TSP). The TSP's of individuals provide information on the extent of the activities they can perform, and gives necessary leads to planners to seek ways to improve them. The analysis of work trips has been carried out to define the TSPs of individuals, their extents and various factors related to the households and the activity location. The household transport vehicle ownership and work travel mode were cross-classified. The results are presented in **Table 3**.

Table 3. Distribution of work trips

Work Travel Mode	No. of Work Trips by Household Head						All Vehicle Ownerships
	Household Vehicle Ownership						
	0	1	2	3	4	5	
0	45	1	10		3	1	60
2			1				1
3				1			1
4	2				5		7
5	2					1	3
6	1						1
7	21		3		3		27
All Modes	71	1	14	1	11	2	100

Table 4. Attributes of the activity work

Work Travel Mode	Average Distance to Work (km)						All Vehicle Ownerships
	Household Vehicle Ownership						
	0	1	2	3	4	5	
0	0.3		0.4				0.3
2			3.0				3.0
3				1.0			1.0
4	4.0				3.3		3.5
5	16.5					250.0	94.3
6	8.0						8.0
7	29.1		13.3		39.3		28.5
All Modes	9.5		3.4	1.0	12.2	125.0	11.1
Work Travel Mode	Average Travel Time to Work (min)						All Vehicle Ownerships
	Household Vehicle Ownership						
	0	1	2	3	4	5	
0	6		11				6
2			30				30
3				10			10
4	15				10		11
5	40					240	107
6	35						35
7	81		30		55		72
All Modes	30		16	10	20	120	28

A general analysis of **Table 3** shows that, out of 100 households in Hala, a considerable proportion (71%) did not own any transportation vehicle, while about 60% of households used walking as the transport mode for their work trips. The remaining 40% of households used other modes for their work journeys. This provides the starting point of the analysis designed to answer the question "what is the 'basic' TSP of the individuals and how do they try to improve them?" Further analysis on average distance to work and average time for work trips was carried out and the results are presented in **Table 4**. Considering the overall average distance to work (**Table 4**), the average for the mode walking is around 0.3 km (0.186 miles). This means that on an average walking covered the work destinations which were about 0.3 km (0.186 miles) away. Similarly households that did not possess any transportation vehicle (vehicle ownership=0) travelled an average distance of 9.5 km (5.9 miles) for work. This was possible when they used other modes of transportation (modes 4-7). The trend for the average time taken for work trips was different from that for distance. The time taken by households not owning a transport vehicle was above the overall average of 28 min. (**Table 4**). This suggests that on an average these households spent more time than the overall average for the area but travelled a lesser distance. The reason was the availability of transport modes at their disposal. Not owning a transport vehicle forced them to either use public transport or to resort to localised trips. In both cases the overall travel time increased, i.e. the walking time in the case of "walking" as travel mode and the waiting time in the case of using public transport (travel mode 7). All vehicle ownerships codes in **Tables 3** and **4** are same as Travel modes in **Table 2**.

An important point worth mentioning is distance and time for work by households owning tractor trailer (mode 4). Usually these households also own farms and live on the farms so their travel pattern for work depicts a unique pattern. Similarly a different trend is found in distance and time for households owning and travelling by car (mode 5). The distinctive nature of the work trip suggests that the individual may be a driver.

4.6 Basic and Improved Time-Space Prism

The distance and time of travel to work may be used to define the individual time-space prism (TSP). The inclinations of the prism sides are defined on the basis of maximum speed of travel by the individual. The extent of the TSP depends both on the inclinations of prism sides as well as the total daily time budget. This time budget was defined as the overall time available to the individual

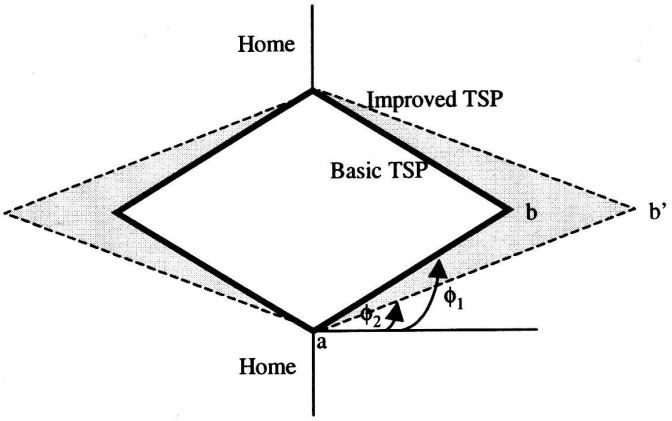

Figure 8. Configuration of individual TSP

between his home coupling constraints, for example fixed timings for leaving and returning home. (Salient elements of TSP of an individual are described in **Figure 1**.)

Figure 8 contains two circumscribed TSPs. The inner TSP is defined as the basic TSP. The inclination of side ab, i.e. the value of the angle 1, is defined on the basis of household vehicle ownership. This is computed using the speed of travel achieved by the individual from a household based on vehicle ownership at household level. The TSP obtained in this way is called basic TSP. The angle 2 defines the inclination of sides ab' of the improved TSP. The improved TSP is computed on the basis of the average speed achieved by the household with a given vehicle ownership using any faster mode of travel. Values of the two angles 1 and 2 in are computed using the following trigonometric relationship:

$$\phi = \tan^{-1}\left(\frac{\text{time}}{\text{distance}}\right) \quad (1)$$

where

ϕ = inclination of the prism boundaries

time = travel time

distance = distance to the activity

Table 5 was used to investigate the effect of various travel modes on the individual TSP. The table uses the data presented earlier in **Table 4** to compute the two values $_1$ and $_2$ using equation (1). For $_1$ (the basic TSP) the time and distance values corresponding to the vehicle ownership group were used (for example Walking for household not owning any transport vehicle). For $_2$ (the improved TSP) the time and distance values used were the overall average for the vehicle ownership group (bottom row in the relevant column). As the data revealed that only household heads are responsible to major source of earning, the data for this individual is only used for this analysis.

Table 5. Basic and improved values of angle phi

Work Travel Mode	Angle phi (degrees)						All Vehicle Ownerships
	Household Vehicle Ownership						
	0	1	2	3	4	5	
0	87.5		87.8				87.6
2			84.3				84.3
3				84.3			84.3
4	75.1				71.7		73.0
5	67.6					43.8	48.5
6	77.1						77.1
7	70.1		66.0		54.4		68.5
All Modes	72.2		78.2	84.3	58.0	43.8	68.4

In **Table 5**, the shaded values in the diagonals of the matrix are the values $_1$ and the shaded values in the 'all modes' row are the corresponding values of $_2$. The analysis of **Table 5** indicates how individuals tend to improve their TSP, as well as accessibility to Work, using the available transport modes. The households with no transport vehicle ownership, for example, would have the basic TSP having inclination of 87.5 degrees, while they improve it up to 72.2 degrees. Similarly, households with ownership of bicycle will improve their TSP from 84.3 degrees to 78.2 degrees. The households with ownership of vehicle types 3 and 5 (tractor trailer and private car, respectively) do not improve their TSP. This is possibly because they are at the maximum value of the inclinations. To generalise, it may be deduced that, all the individuals (belonging to any vehicle ownership category) would either tend to improve their TSP or would at least remain at their basic TSP by switching the mode which is the most feasible. On some higher note this points out the household economics. These findings were in line with the conclusions of Ellis and Hine (1995) that the rural households in Asian countries studied by them made use of the available transport services in order to improve accessibility of economic activities.

4.7 Utilization Index

In household accessibility analysis it may be useful to analyze how much the travel burden effects the overall activity participation, especially economic activity like work.

It means that if proportion of time spent in travelling would be reduced a person could spend the time saved in the economic activity. This leads to development of a time utilization index. Using individual activity participation information, it was possible to analyse the total daily time budget of the individuals as well as the real constraints shaping their TSP. From the individual activity diaries the following information was obtained:

a) start timings for work trips
b) timings for return trips
c) duration and mode for work trips
d) distance and duration of work

Table 6 summarizes the information on (a) and (b). It contains the average time of start of work trips, as well as the average time for start of journey to home. The clusters refer to various survey areas covered in detailed field survey carried out as part of this research. The column 'count' is the number of individuals observed in the given cell. It was found that the majority of the individuals left home for work at 08:00 (in the case of clusters 2, 4 and 5) or 08:30 (in the case of clusters 1 and 3). Similarly the majority of the individuals started the journey from work to home at 14:00 (in the case of cluster 2), 15:00 (in the case of clusters 1, 3 and 5), or 14:45 (in case of cluster 4). This leads to the conclusion that there is a set starting time for journeys to and from work. This pattern revealed that:

i) as far as work trips were concerned, the rural population either did not possess or did not exercise various varieties of work options (for example working from home)
ii) the mass out-going and in-coming timings showed some sort of dependency on external factors (for example connection to public transport).

Table 6. Work trip timings statistics

Cluster1			**Cluster2**			**Cluster3**			**Cluster4**			**Cluster5**		
Leaving hme for work			Leaving hme for work			Leaving hme for work			Leaving hme for work			Leaving hme for work		
Slot	Time	Count	Slot	Time	Count	Slot	Time	Count	Slot	Time	Count	Slot	Time	Count
10	8:30	62	8	8:00	18	9	8:15	1	4	7:00	4	8	8:00	21
11	8:45	2	9	8:15	2	10	8:30	52	8	8:00	18	12	9:00	2
28	13:00	3	10	8:30	7	22	11:30	6	9	8:15	2	29	13:15	2
Return hme for work			Return hme for work			Return hme for work			Return hme for work			Return hme for work		
Slot	Time	Count	Slot	Time	Count	Slot	Time	Count	Slot	Time	Count	Slot	Time	Count
36	15:00	66	32	14:00	25	9	8:15	5	2	6:30	2	6	7:30	3
40	16:00	3	48	18:00	3	35	14:45	5	35	14:45	23	32	14:00	1
52	19:00	21	49	18:15	6	36	15:00	59	56	20:00	10	36	15:00	23

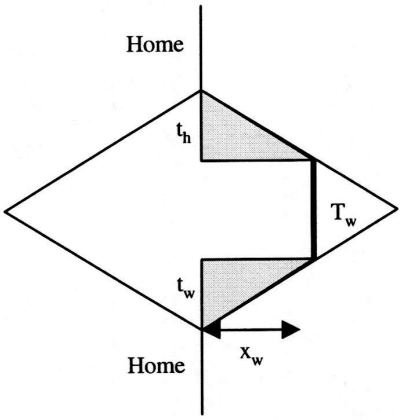

Figure 9. TSP of working individuals

Based on the above information it can be deduced that the individuals have a fixed time budget as far as work trips are concerned. This concept was used to define a simplified time-space prism for working individuals, as shown in **Figure 9**. It is assumed in **Figure 9** that.

a) the individual only takes part in the activity Work
b) the activity Work has a fixed duration of time Tw
c) trips to and from work have equal duration, such that tw=th
d) distance to work is given by xw, and
e) total time budget of the individual comprises of the above-mentioned three time durations

From the above conceptual setting, and considering that the individual needs to travel to access the activity work, a mathematical relationship can be developed as:

$$TW = t_w + T_w + t_h \tag{2}$$

where

TW = total time spent to access the activity work

t_w = travel time to work

t_h = travel time from work

T_w = actual work duration

Considering that the time for travel is unutilised, a utilisation index can be developed so as to analyse the effect of time of travel for work trips. From the utilisation index can be defined as the non-shaded area in the total time budget. Mathematically, it can be given as the proportion of the total access time spent in travelling, i.e.:

$$UI = \frac{T_w}{TW} \tag{3}$$

where

UI = utilisation index

The utilisation index gives the percentage of time utilised when an individual accesses the work location. This is based on the variation in the shaded area, which represents unutilised time. The above idea was explored using the data on distance to work from the five clusters of Hala. Considering that the distance people have to travel to reach Work locations was a major factor affecting the utilisation of time for activity participation, an analysis was carried out to study the relationship between distance to Work location and the UI. The average value of the travel distance to Work was found to be 11 km (6.84 miles). Two subgroups of household heads were formed on the basis of this threshold value; i.e. persons with travel distance to work below and above the average distance of 11 km (6.84 miles). Two graphs (**Figure 10**) show how the distance to Work affects the utilisation index, with respect to the average travel distance threshold of 11 km (6.84 miles). This was also confirmed by testing of relationship between Distance and Utilization Index by running correlation between the two variables (**Table 7a**).

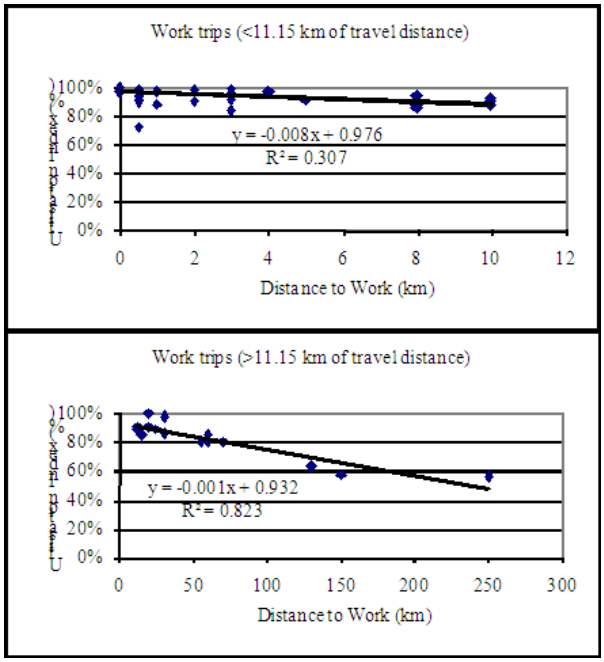

Figure 10. Effect of household income on utilization index

Table 7a. Testing of Relationship between Distance and Utilization Index

Correlation Coefficient Between Distance and Utilization Index	
Distance	**Corr.Coeff.**
<=11km	-0.55
>11km	-0.91

On the basis of **Figure 10** and **Table 7a** it can now be deduced that work trips within a distance of 11 km (6.84 miles) (average for the area) do not seem to affect the utilisation index. This is logical, as the average distance below certain values may not create a significant deterrence. Travel distances higher than 11 km (6.84 miles) (**Figure 10**) play an important role in affecting the time utilisation. This happens because the individuals spend a considerable time in travelling to reach the activity, which, in turn, decreases the overall time for participation in activity Work. When the relationship between household income and distance to work was studied, it was found that an increase in household income is not a direct result of travelling long distances. This was done by computing correlation coefficients between Distance to Work and Household Income. **Table 7b** depicts that no correlation exists between the two, for both subgroups of the population (less and greater than 11km (6.84 miles)). This indicates that in rural areas of Pakistan, Household Heads have to travel longer distance to earn their livings, irrespective of a direct increase in their income.

On the basis of the above analysis it can be deduced that the distance to work, beyond a certain threshold value, has as a profound effect in reducing utilisation of time for earning activities. The threshold may be defined as the average travel distance for the given area. The analysis is an example of the use of time geography to study household economics of decision-making. The decision to take part in distant work activities does not necessarily result in increasing the household income, it may just be the effect of the limited opportunities available within the village that the population has to travel longer distances at the cost of reduction in their overall time utilisation.

Table 7b. Testing of Relationship between Distance and Household Income

Correlation Coefficient Between Distance and Household Income	
Distance	**Corr.Coeff.**
<=11km	0.10
>11km	0.32

5. CONCLUSIONS

This paper demonstrated the application of time geography approach to rural transportation planning in developing countries. A concept of basic and improved time-space prism (TSP) has been developed. The spatial separation of activities defines the trip distribution for personal travel. In the case of rural areas of developing countries, there are discrete locations of activities fulfilling most needs and services and the choice of locations is therefore limited. For example in Pakistan, people from all villages within about 20 km (12.43 miles) travel to Hala (Sindh Province) for shopping, hospital, banking and postal services. This results in a multitasking environment for activity participation. In this case, trip distribution is not primarily based on the choice of location, but on the allocation of time for various activities. This becomes the basis of defining origin and destination of various travel decisions throughout the day.

In rural areas of many developing countries especially in Pakistan, personal travel is mostly carried out on public / community transport facilities. Most of the village access roads are un-engineered tracks. The transport service providers who operate on these tracks set-up their fares on the basis of their operating cost. In turn, the choice of travel mode is highly dependent on the ability of the household to use the available facilities. In quantifying travel mode choice it is important to consider the need for travel, the household socio-economics to afford a transport mode and the extent of the transportation infrastructure in place.

It was found that distance to work, beyond a certain threshold value, has as a profound effect in reducing utilisation of time for earning activities. The threshold may be defined as the average travel distance for the given area. The analysis is an example of the use of time geography to study household economics of decision-making. The decision to take part in distant work activities is not necessarily based on increasing the household income, it may just be the effect of the limited opportunities available within the village that the population has to travel longer distances at the cost of reduction in their overall time utilisation.

It can be deduced from the above analysis that in the limited time-budget situation, the distance to Work affects the overall time available for earning activities. The development policies designed to address the mobility problems of long distance commuters would therefore be expected to yield a high impact.

It was argued that households use a number of ways so as to improve their TSPs in order to bring more activities within their reach. The analysis confirmed that technological developments when trickled down to individuals may be able to enhance their mobility and, as a result, their accessibility to various opportunities.

The concepts developed provide a basis for development of travel demand models considering access to services as the primary utility while using the time geography approach for mathematical formulation of the problem. This may provide a way ahead for improved vision of transportation interventions in the overall context of improved accessibility to activities increasing earning/well being of the society.

ACKNOWLEDGEMENT

This paper is published out of the work carried out by the Author for his Ph.D research, at the University of Birmingham, UK, fully funded by Government of Pakistan. The supervision and support by Professor Dr. Henry Kerali and Dr. Jennaro Odoki (Sr. Lecturer), and the help of persons and organisations who provided support for field data collection from Pakistan, are all duly acknowledged.

The painstaking job of referees to the original manuscript is greatly acknowledged as being the prime source of the improved version of the final manuscript.

REFERENCES

[1] Hagerstrand T. What about people in regional science. Regional science association papers XXIV, 1970. p. 7-21.

[2] Miller JH. Measuring Space-Time Accessibility Benefits within Transportation Networks: Basic Theory and Computational Procedures. Geographical Analysis 1999,31:187-212.

[3] Ali MS. Accessibility-Activity Based Approach To Model Rural Travel Demand In Developing Countries. PhD thesis. University of Birmingham, UK, 2001.

[4] Nehra RS Modeling Time Space Prism Constraints in a Developing Country Context, MSc thesis. University of South Florida, 2004.

[5] Ali MS, Adnan M. An Approach for Modelling Travel Decision Economics for Rural Areas of Developing Countries. In: Proceedings of WCTR'04 10 World Conference on Transport Research. Istanbul, Turkey: 2003.

[6] Ali MS. Travel Behaviour Analysis in Developing Countries Using Time-Space Prism Approach. In: Proceediongs of 7th ICCE. Tehran, Iran: 2006.

[7] Burns L. Transportation, Temporal and Spatial Components of Accessibility. Lexington Books, Massachusetts, 1979.

[8] Odoki J. Accessibility-Benefits Analysis As A Tool For Transportation Planning In Developing Countries. PhD Thesis, University of Trieste, Polytechnic of Milan, Italy, 1992.

[9] Odoki JB, Kerali HR, Santorini F. An Integrated Model for Quantifying Accessibility-Benefits in Developing Countries. Transportation Research – An International Journal, Part A Policy and Practice 2001; 35A(7):601–623.

[10] Ali MS, Odoki JB, Kerali HR. An Accessibility-Activity Based Approach to Model Rural Travel Demand in Developing Countries. In: Proceedings of XXII PIARC World Road Congress. Durban, South Africa: 2003.

[11] Jones P, Dix M, Clarke M, Heggie I. Understanding Travel Behaviour. Gower, England, 1983.

[12] Ben-Akiva M, Bowman JL, Gopinath D. Travel Demand Model System For The Information Era. Transportation 1996;23:241-266.

[13] Wu YH, Miller HJ. Computational Tools for Measuring Space-Time Accessibility within Dynamic Flow Transportation Networks. Journal of Transportation and Statistics 2001;4(23):1-14.

[14] Pendyala RM, T Yamamoto, Kitamura R. On The Formulation of Time-Space Prisms to Model Constraints on Personal Activity-Travel Engagement, Transportation 2002;29:73–94.

[15] Mei-Po K. Analysis of Human Spatial Behavior in A GIS Environment: Recent Developments and Future Prospects. Journal of Geographical Systems 2000;2:85-90.

[16] Miller HJ, Wu YH. GIS Software for Measuring Space-Time Accessibility in Transportation Planning and Analysis. Geoinformatica 2000;4(2):141-159.

[17] Howe J. Transport for the poor or poor transport? IHE Working paper IP-12, International Institute for Infrastructural, Hydraulic and Environmental Engineering, Delft University, The Netherlands.

[18] Edmonds G. Wasted time: The Price of Poor Access. RATP No.3, ILO-Geneva, 1998.

[19] Bryceson D, Howe J. African Rural Household and Transport: Reducing the Burden on Women. IHE Working paper IP2, International Institute for Infrastructural, Hydraulic and Environmental Engineering, Delft University, The Netherlands, 1992.

[20] Ellis S. The Economics Of The Provision Of Rural Transport Services In Developing Countries. PhD Thesis. Cranfield University, 1996.

[21] Howe J. Enhancing Nonmotorized Transportation Use In Africa - Changing The Policy Climate. Transportation Research Record 1487, Transportation Research Board., Washington, 1995.

TENSILE BEHAVIOR CHANGE DEPENDING ON THE VARYING TUNGSTEN CONTENT OF W–NI–FE ALLOYS

Syed Humail Islam[1], Farid Akhtar[2], Syed Jawaid Askari[2], Muhammad Tufail Jokhio[1], Xuanhui Qu[2]

ABSTRACT

Tungsten heavy alloys (WHAs) are metal–metal composites consisting of nearly pure spherical tungsten particles embedded in a Ni–Fe–W or Ni–Co–W or Ni–Cu–W ductile matrix. In this dual phase alloy, there are several complicated relations between the ductile matrix and hard tungsten particles. The aim of this research was to examine the effect of varying tungsten content on the microstructure and mechanical properties of tungsten heavy alloys. The microstructural parameters (grain size, connectivity, contiguity and solid volume fraction) were measured and were found to have a significant effect on the mechanical properties of tungsten-based heavy alloys. The result shows that the binding strength between the W and the matrix phase has a major influence on the ductility of tungsten-based alloys. The larger this binding force is, the better the ductility is.

Keywords: Tungsten heavy alloys; mechanical properties; microstructure; fracture morphology

1. INTRODUCTION

Tungsten heavy alloys are two phase composites consisting of nearly pure tungsten grains dispersed in a low melting temperature ductile matrix of other metals such as iron (Fe), nickel (Ni), cobalt (Co), or copper (Cu) [1,2]. The typical mean tungsten grain size varies from 20 μm (66 μft) to 60 μm (197 μft) depending on the initial particle size, volume fraction of tungsten, sintering temperature, and sintering time. Due to their high density and high strength associated with the bcc tungsten phase, and high ductility attributed to the fcc matrix, these alloys are used in application such as kinetic energy penetrators, radiation shielding, counter balance, vibrational damping devices, and other military and civil applications [3,4].

During the last two decades, the research of tungsten heavy alloys has concentrated on strengthening methods, which do not compromise their density. This is especially important in military applications. The combination of a powder with a particular microstructure and a consolidation technique that can maintain that microstructure is an effective method for obtaining bulk samples with a unique microstructure. The mechanical properties of tungsten heavy alloys are determined by various factors; in particular, the strength of W/W and W/matrix interfaces [5]. Microstructural factors, such as tungsten particle size, matrix volume fraction and tungsten–tungsten contiguity, affect the mechanical properties of tungsten heavy alloys [6]. The main focus of this study is to investigate

[1] *Department of Industrial and Manufacturing Engineering, NED University of Engineering and Technology Karachi 75270, Pakistan*

[2] *School of Materials Science and Engineering, State Key Laboratory for Advanced Metals and Materials, University of Science and Technology Beijing, Beijing 100083, PR China*

(Reproduced with the permission of Elsevier)

Syed Humailul Islam is an Associate Professor in the Department of Industrial and Manufacturing Engineering at NED University of Engineering and Technology, Karachi, Pakistan. He received his Beng and MEng in Mechanical Engineering in 1998 and 2003, respectively. He received his PhD in Materials Science and Engineering from the University of Science & Technology Beijing, China in 2007.

Farid Akhtar received his Beng in Metallurgical and Materials Engineering and MEng in Materials Engineering in 1999 and 2002, respectively. He received his PhD in Materials Science and Engineering from the University of Science & Technology Beijing, China in 2007. His research interests include powder metallurgy science, particularly in alloy design for sintering, infiltration and rapid manufacturing of aluminium and titanium systems

Syed Jawaid Askari received his BEng and MEng in Mechanical Engineering in 1990 and 1994, respectively. He received his PhD in Materials Science and Engineering from the University of Science & Technology Beijing, China in 2007. His research interests include an investigation of the processing, structure, and mechanical property characterization of diamond films grown using a variety of deposition conditions and substrate materials.

Muhammad Tufail Jokhio received his BEng in Mechanical Engineering and MEng in Manufacturing Systems in 1991 and 1994, respectively. He received his PhD in Mechanical Engineering from University of Nottingham in 1999. His research interests include Development of Composite Materials

Xuanhui Qu received his BEng and MEng in Metallurgical Engineering in 1984 and 1986, respectively. He received his PhD in Materials Science and Engineering from the Central South University Changshaw, China in 1992. His research interests include Development of Part by Powder Metallurgy and Powder Injection Moulding Techniques

and identify trends in microstructure behaviour relative to variations in W content and the influence of microstructure change on the mechanical properties of tungsten heavy alloys.

2. EXPERIMENTAL DETAIL

Elemental powders of tungsten, nickel and iron were mixed to produce tungsten heavy alloys with compositions of 88%, 93% and 95 wt% of tungsten with Ni:Fe in the ratio of 7:3. **Table 1** summarizes the characteristics of the powders. The powders were consolidated into green compacts with 55–65% of theoretical density by die pressing. The green compacts were liquid phase sintered at a temperature of 1500 ^{o}C (2732^{o}F) for 30 min and in hydrogen atmosphere. The sintering cycle followed for all experiments was 10 ^{o}C/min (50 ^{o}F/min) up to 800 ^{o}C (1472^{o}F) and 5 ^{o}C/min (41^{o}F/min) thereafter. During the cooling cycle, at 1400 ^{o}C, the atmosphere changed from hydrogen to argon. The sintered samples were subsequently annealed in a vacuum at a temperature of 1100 ^{o}C (2012^{o}F) for 8 h, in order to reduce the content of absorbed hydrogen and prevent embrittlement, and then water quenched to circumvent the impurity segregation problem. The densities of the sintered specimens were measured by the Archimedes water immersion method. Quasi-static tensile testing was carried out using an Instron testing system with a constant cross head displacement rate of 0.5 mm/min (0.02in./min) in ambient air at room temperature. Three specimens were used for each measurement. Samples were prepared for microstructural evaluation by cutting, mounting, grinding and polishing to a 0.3 ìm (0.98 µft) surface finish using standard metallographic procedures. The size of the tungsten particles, the volume fraction of the matrix phase, the connectivity and tungsten–tungsten contiguity of the sintered tungsten heavy alloys were characterized using LEO-1450 SEM (scanning electron microscope). The volume fraction, connectivity and contiguity were measured manually by point counting method. Fractographical observations of tensile tested specimens were conducted by LEO-1450 SEM.

Table 1. Characteristics of Ni, W and Fe Powder

Powder	W	Ni	Fe
Purity	99.2%	99.6%	99%
Shape	Irregular	Spiky	Nearly spherical
Particle size (μm)			
D_{10}	3.1	4.3	1.9
D_{50}	7.6	14.6	3.4
D_{90}	19.1	33.5	6.3
Apparent density (g/cm^3)	4.3	3.1	2.6
Tap density (g/cm^3)	6.3	3.6	4.1
Surface area (m^2/cm^3)	1.138	0.734	2.236

3. RESULTS AND DISCUSSION

3.1 Microstructure

The microstructures of heat treated alloys containing 88%, 93% and 95% weight tungsten are presented in **Figure 1a–c**. As can be seen, the tungsten particles in Figure 1a are smaller and rounder than those in Figures 1b and c. The difference is attributable to the difference in the amount of matrix phase present in each alloy. In 88 wt% tungsten alloys, there is a greater amount of matrix phase available which promotes the Ostwald ripening and results in smaller and rounder grains. The difference in size between the particles in Figures 1b and c is also attributable to the difference in the amount of matrix phase present in each alloy. In Figures 1b and c the tungsten particles are very irregular in shape. It is important to note that this irregularity increases the contact area of the tungsten–matrix interphase, thereby considerably increasing the strength of the alloys [7].

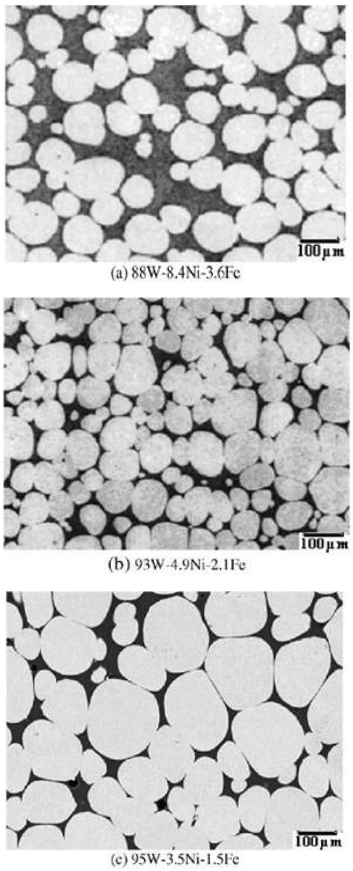

Figure 1. Microstructure of WHAs sintered at 1500°C (2732°F) for 30 min and vacuum annealed at 1100°C (2012°F) for 8 h.

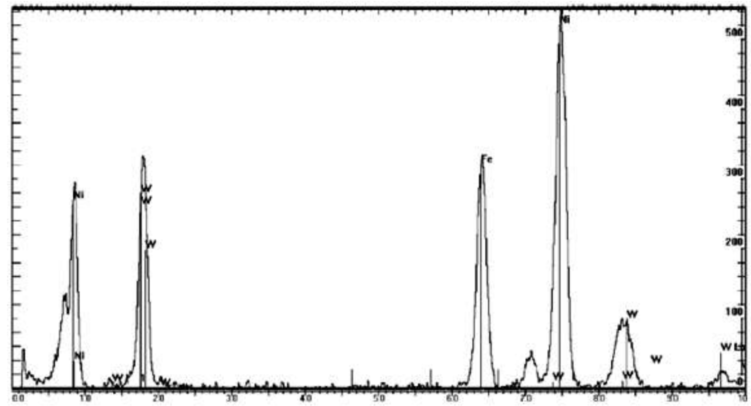

Figure 2. EDX spectrum of matrix phase in 93W-4.9Ni-2.1Fe

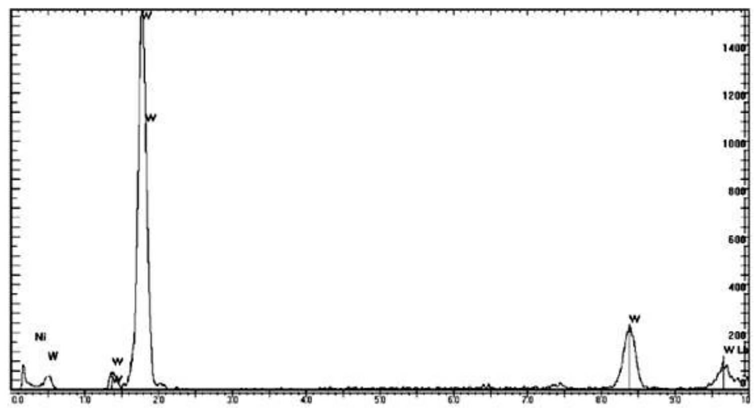

Figure 3. EDX spectrum of matrix phase in 93W-4.9Ni-2.1Fe

Quantitative EDX analysis showed that W–Ni–Fe matrix phase consists of about 24wt%W–22wt%Fe–54%Ni in 93%W. **Figure 2** shows the EDX spectrum of matrix phase of 93 wt%W. **Figure 3** shows the EDX spectrum for the tungsten phase which showed imperceptible presence of iron and nickel making it pure tungsten phase. Interestingly, the compositions of matrix phase of 88% and95%Ware not very different from the 93%W.

The microstructure measurements of grain size, solid volume fraction, contiguity and connectivity are taken from SEM micrographs. There is a major change in microstructure as the tungsten content increases from 88% to 95 wt%. The measured volume fraction of the tungsten grains increases linearly from 0.73 for the 88%W alloy to approximately 0.91 for the 95%W alloys. **Figure 4** shows the variation of tungsten grain size, contiguity and two dimensional connectivity with the increase of tungsten content in the alloy composition from 88% to 95 wt% sintered at 1500 ^oC (2732^oF) and vacuum heat treated at 1100 ^oC (2012^oF) for 8 h. It is important to note that not only contiguity but also connectivity, tungsten grain size and matrix volume fraction is largely affected by the tungsten content.

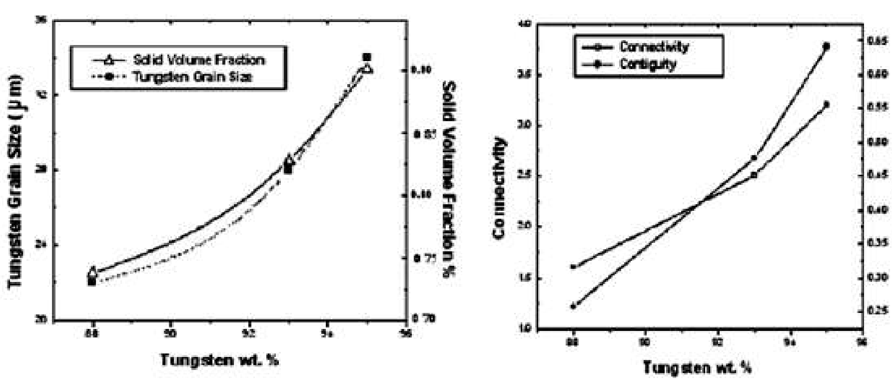

Figure 4. Solid volume fraction, contiguity, connectivity and grain size variations with sintering temperature for 88%, 93% and 95% tungsten.

Table 2. Tensile properties of 88%, 93% and 95% W-based heavy alloys sintered at 1500 °C for 30 min and vacuum annealed at 1100 °C for 8 h

Mechanical properties/composition	88W-8.4Ni-3.6Fe	93W-4.9Ni-2.1Fe	95W-3.5Ni-1.5Fe
Density (g/cm^3)	16.60	17.52	17.98
Tensile strength (MPa)	894	996	916
Elongation (%)	30	23	11

3.2. Tensile Properties

The mechanical properties shown in **Table 2** can be explained by considering the effect of tungsten content on alloy strengthening. **Table 2** shows that the tensile strength of the 93 wt% tungsten is higher than the 88% and 95 wt% tungsten-based alloys. This is first because of the tungsten content and the size of the tungsten particles after sintering and heat treatment. Secondly, uniform distribution of the matrix phase and the tungsten particles appear to be well bonded to the Ni–Fe–W matrix. However, at the same time, the ductility of the alloy decreases as the tungsten content is increased, and above 93%W the ductility of the alloys decreases drastically. This in turn causes the tensile strength of the alloys to decrease at above 93%. This phenomenon is attributable to a higher number of W–W grain boundaries at high contiguities which are the weakest interfaces. Though alike in some aspects, the microstructures of the three alloys are different enough to present a range of mechanical properties. At lower tungsten content (88%W), the higher ductility is a result of lower contiguity and connectivity, the availability of more matrix phase and the uniform distribution of the matrix phase between the tungsten particles. At higher tungsten content (95%W), the ductility of the alloys decreases noticeably because of higher contiguity and connectivity, as the tungsten–tungsten particle interfaces are the most brittle parts. These interfaces split easily and micro cracks soon appear even at very low load, acting as fracture sites and helping easy crack propagation because the amount of matrix phase available is not sufficient to arrest the proliferation of these cracks. Thus, they cause deterioration of the overall properties of tungsten heavy alloys. Important thing is to deal with the matrix phase inconsistency by properly control the grain growth of the tungsten particle during the sintering process.

3.3. Fracture Morphology

Scanning electron micrographs (QBSD) of the fracture surfaces of alloys containing 88%, 93% and 95% are shown in **Figure 5**. The W grains appear light and the matrix phase appears darker in these pictures. It is well known that there are four possible fracture paths [8] for the heavy alloy microstructure: matrix failure, W cleavage, W–W intergranular failure and W–matrix interfacial separation. By investigating the fracture surfaces, differences in the mechanisms of fracture in the 88%, 93% and 95 wt%. W alloys are readily observable and these indicate that the fracture behaviour and tensile properties of the tungsten heavy alloys are strongly influenced by the variation in the tungsten content of the alloy. In **Figure 5a**, the intergranular cleavage and fracture, separation of W–W facets, W–matrix decohesion, and isolated matrix rupture is visible for 95 wt% W alloys. **Figure 5b** shows that the processing method used in this study resulted in a strong interface, as evidenced by excellent W–matrix adhesion and a minimum amount of interfacial separation in the 93 wt%W alloys. The other three failure modes can also be observed on the fracture surfaces; however, the proportion of each feature depends upon W content. The amount of W–W separation is high in the case of the 95%W, whereas the amount of W cleavage is much greater for 88 wt% alloy. A close examination of the fracture surfaces reveals several interesting phenomena. For example, it appears that W cleavage occurs more frequently in larger W grains. The amount of W–W grain boundary failure is fairly uniform over the three different compositions of the alloy. These results further confirm that the W–W grain boundary is the weakest interface since all fracture surfaces exhibit approximately the same amount of failure by this path. The 95%W tensile tested samples show predominantly intergranular fracture (**Figure 5a**). This is expected, because the low volume fraction of binder ensures a high degree of contiguity and higher contiguity helped in microcrack nucleation. As the W content is reduced, the fracture develops into a cleavage in the W grains, and is commonly observed in this type of alloy [9–11]. SEM images of the 88%W, as shown in **Figure 5c** and **d**, reveal partial W–matrix separation, cracks in W due to its brittle quality and thin areas of matrix between W grains. **Figure 5d** shows that tensile failure of the 88% alloy

starts by separation of W/W and develops by producing cleaved tungsten grains after strain hardening the matrix and then matrix rupture occurs. Failure of the strain-hardened matrix around the smaller W grains is evident in this alloy, as shown in **Figures 5e** and **f**. The higher the ductility, the greater is the proportion of W cleavage and matrix phase failure. Also, decohesion of the W–matrix interphase is evident with low ductilities. This study also shows that crack formation in the tungsten heavy alloy mostly starts principally through W–W interfaces rather than through interfaces between W grains and the matrix phases. The matrix phase plays an important role in hindering crack propagation. For a fixed contiguity, the ductility depends on the W matrix interfacial properties. These results show that the binding strength between the W and the matrix phase has a major influence on the ductility of tungstenbased alloys. The larger this binding force is, the better the ductility.

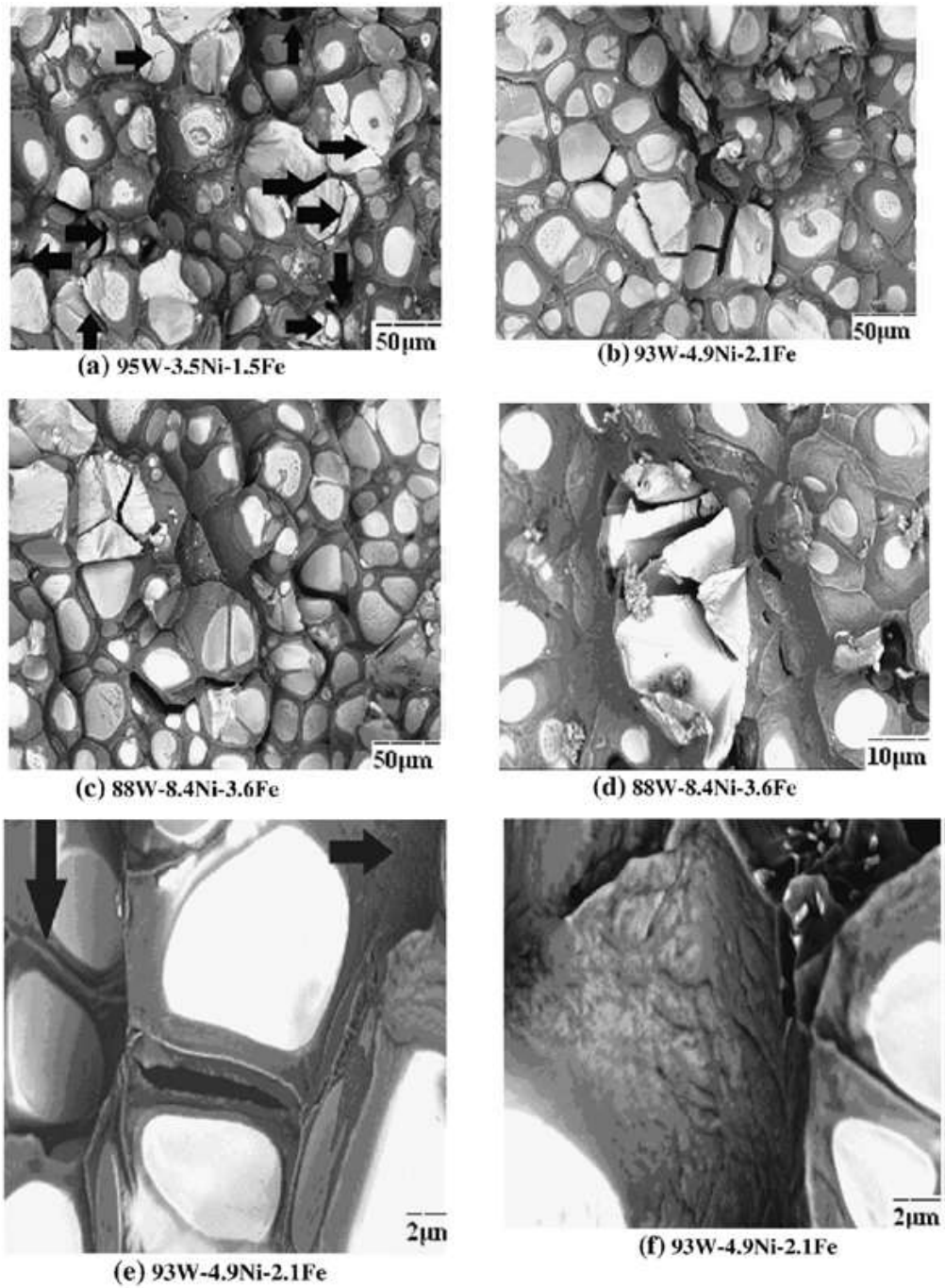

Figure 5. Fracture morphology of WHAs sintered at 1500°C (2732°F) for 30 min and vacuum annealed at 1100°C (2012°F) for 8 h.

4. CONCLUSIONS

This study has determined the variation in mechanical properties associated with different compositions and microstructural parameters of tungsten heavy alloys produced by die pressing and liquid-phase sintering. The inherent property of tungsten at various compositions does not change. The variation in mechanical properties at three different compositions is a result of the difference in tungsten grain size, matrix volume fraction and weak W–W contiguity. Good cohesion between tungsten and the matrix results in a material that is capable of transferring the stresses between W grains and the matrix. The crack formation is attributable to tensile force acting on poorly bonded areas. The ultimate tensile strength is at a maximum at 93%W and this is because of optimal tungsten grain size, better bonding energy between tungsten and the matrix, and a homogeneous distribution of the matrix phase.

REFERENCES

[1] Upadhyaya A. Processing strategy for consolidating tungsten heavy alloys for ordnance applications. Mater Chem Phys 2001;67:101–110.

[2] Ryu HJ, Hong SH, Baek WH. Microstructure and mechanical properties of mechanically alloyed and solid state sintered tungsten heavy alloys. Mat Sci Eng A 2000;291:91–6.

[3] Cai WD, Li Y, Dowding RJ, Mohamed FA, Lavernia EJ. Rev Particulate Mater 1995;3:71.

[4] German RM. Critical developments in tungsten heavy alloys. In: Bose A, Dowding RJ, editors. Tungsten and tungsten alloys. Princeton (NJ): MPIF; 1992. p. 3–13.

[5] Noh JW, Kim EP, Song HS, Baek WH, Churn KS, Kang SJL. Matrix penetration of W/W grain boundaries and its effect on mechanical properties of 93W–5.6Ni–1.4Fe heavy alloy. Metall Trans A 1993;24:2411–6.

[6] Rabin BH, German RM. Microstructure effects on tensile properties of tungsten–nickel–iron. Metall Trans A 1988;19:1523–32.

[7] Hong MH, Kim EP, Baek WH, Moon IH. The effect of manganese addition on the microstructure of W–Ni–Fe heavy alloy. Metall Mater Trans A 1999;30A:627–32.

[8] German RM, Churn KS. Sintering atmosphere effects on the ductility of W–Ni–Fe heavy metals. Metall Trans A 1984;15A:747–54.

[9] Gero R, Borukhin L, Pikus I. Some structural effects of plastic deformation on tungsten heavy metal alloys. Mat Sci Eng A 2001;302:162–7.

[10] Rabin BH, Bose A, German RM. Characteristics of liquid phase sintered tungsten heavy alloys. Int J Powder Metall 1989;25:21–7.

[11] O'Donnell RG, Woodward RL. The composition and temperature dependence of the mechanical properties of tungsten alloys. Metall Trans A 1989;21:744–8.

AN INVESTIGATIVE STUDY OF THE INTERFACE HEAT TRANSFER COEFFICIENT FOR FE MODELLING OF HIGH SPEED MACHINING

Syed Amir Iqbal[1], Paul T Mativenga[2], Mohammad A Sheikh[2]

ABSTRACT

This paper is concerned with the development of an experimental setup and Finite Element (FE) modelling of dry sliding of metals to estimate interface heat transfer coefficient. Heat transfer between the chip, the tool, and the environment during the metal machining process has an impact on temperatures, wear mechanisms and hence on tool-life and on the accuracy of the machined component. For modelling of the metal machining process, the interface heat transfer coefficient is an important input parameter to quantify the transfer of heat between the chip and the tool and to accurately predict the temperature distribution within the cutting tool. In previous studies involving FE analysis of metal machining process, the heat transfer coefficient has been assumed to be between 10-500 kW/m^2 ^{o}C (0.49-24.5 BTU/sec/ft^2/^{o}F), with a background from metal forming processes (especially forging). Based on the operating characteristics, metal forming and machining processes are different in nature. Hence there was a need to develop a procedure close to metal machining process, to estimate this parameter in order to increase the reliability of FE models. To this end, an experimental setup was developed, in which an uncoated cemented carbide pin was rubbed against a steel workpiece while the later was rotated at speeds similar to the cutting tests. This modified pin-on-disc set-up was equipped with temperature and force monitoring equipment. A FE model was constructed for heat generation and frictional contact. The experimental and modelling results of the dry sliding process yield the interface heat transfer coefficient for a range of rubbing speeds.

Keywords: High Speed Machining, frictional contact, Interface heat transfer coefficient

1. INTRODUCTION

The work done to plastically deform and shear away workpiece material during the machining process is largely converted into heat. O'Sullivan D, Cotterell M. Temperature Measurement in Single Point Turning. J Materials Processing Technology 2001;118:301-308. This heat energy increases the temperatures of the chip, the tool and the machined surface. A very small amount of this heat energy is dissipated to the environment. The second largest source of heat generation during the machining process for cases where undeformed chip thickness is far greater than the tool edge radius has been identified as the frictional heat source in the secondary deformation zone. As a result, heat flows from the chip to the tool rake face and a thermal contact exists between these contacting surfaces. This heat transfer between the chip, the tool and the environment has an impact

[1]*Department of Industrial and Manufacturing Engineering, NED University of Engineering & Technology, Karachi, Pakistan, Ph. +92-21-9261261-68, Fax. +92-21-9261255, Email: syed_a_iqbal@yahoo.com,*

[2]*Manufacturing and Laser processing Group, School of Mechanical, Aerospace and Civil Engineering, The University of Manchester, Manchester, UK*

(Reproduced with the permission of Proceedings of the Institution of Mechanical Engineers, Part B: Journal of Engineering Manufacture)

Syed Amir Iqbal received his PhD in modeling of High Speed Machining Process from the University of Manchester in 2008, under the joint supervision of Drs Mativenga and Sheikh. He has published articles on tool-chip contact and interface phenomena at high cutting speeds.

Paul T Mativenga received his PhD in High speed machining from The University of Liverpool in 2001. Since 2002, he has held a lecturing post at UMIST and then subsequently the University of Manchester. He leads a large research group investigating thin film tool coatings, micromachining and high speed machining and has published widely on these topics. He is a Principal Investigator on an active DTI/EPSRC extend life micro tooling project.

Mohammad A Sheikh received his MSc and PhD from University of Sheffield in 1978-1983. He is Currently a senior Lecturer in the University of Manchester. He has vast experience in the field of mechanical damage and thermal transport analysis of composites, computer aided modeling of materials in manufacturing, modeling of laser process and machining.

on temperatures, wear mechanisms and hence on tool life and accuracy of the machined surface. The heat transfer at the tool-workpiece interface is commonly assumed to be governed by the interface heat transfer coefficient. The interface heat transfer coefficient *h* can be defined by Eq. 1 as shown below:

$$h = \frac{q}{\Delta T} \tag{1}$$

where q is the average heat flow across the interface and ΔT is the temperature drop. It has been established that interface heat transfer coefficient is a function of several parameters, the dominant ones being contact pressure, interstitial materials, macro and micro geometries of the contacting surfaces, temperature and the type of lubricant or containment and its thickness [2].

For the FE modelling of metal machining processes, the boundary conditions at the tool-chip interface are usually formulated in terms of the interface heat transfer coefficient. Thus, the interface heat transfer coefficient is an important input parameter to quantify the transfer of heat between the chip and the tool, and to accurately predict the temperature distribution within the cutting tool. In all the previous work on FE modelling of metal machining process, the numerical values used for defining interface thermal boundary condition were taken from metal forming processes (mostly metal forging). A discussion is presented in this paper regarding the differences in the nature and operating characteristics of machining and forging processes. It is concluded from this discussion that there is a need to develop a procedure close to metal machining process, to estimate this parameter in order to increase the reliability of FE models. Due to experimental difficulties in measuring temperature at the tool chip interface, a new method for estimating values of interface heat transfer coefficient is presented. It is based on a simplified setup of two body heat transfer with the amount of heat generated in the rubbing process depending on the rotational speed. The interface heat transfer coefficient for this sliding contact scenario is predicted by using FE modelling approach.

2. EXISTING SCENARIO FOR INTERFACE HEAT TRANSFER COEFFICIENT VALUES IN MACHINING SIMULATIONS

In the application of interface heat transfer coefficient to the chip formation simulations, very high values of '*h*' have been used based on the assumption of perfect contact. Yen et al. [3] used a very high value (value not mentioned) of interface heat transfer coefficient to study the effect of tool geometry on orthogonal machining process, assuming perfect contact between the chip and the tool. In another study, Yen et al. [4] again used a very high value of interface heat transfer coefficient (value not reported) to model tool wear in orthogonal machining, again for perfect contact. To simulate orthogonal machining process using coated tools, again assuming perfect thermal contact between the tool and the chip, Yen et al. [5] used a value of 100 $kW/m^2\,^oC$ (4.89 $BTU/sec/ft^2/^oF$) for the interface heat transfer coefficient. The workpiece material used was AISI 1045 steel with tungsten carbide tool, coated with different coatings at a cutting speed of 220 m/min (722 ft/min). Klocke et al. [6] also assumed a very high value of interface heat transfer coefficient between the tool and the chip for orthogonal machining of AISI 1045 steel with a ceramic tool at ultra high

Table 1. Summary of Interface Heat transfer coefficient values used for machining simulation

Researcher	Workpiece material	Tool material	h(kW/m^2 ^{o}C)
Yen et al [3]	AISI 1020	Uncoated WC	**
Yen et al [4]	AISI 1045	Tic/Al_2O_3/Tin coated WC	100
Yen et al [5]	AISI 1045	Uncoated WC	100
Klocke et al [6]	AISI 1045	SiC-Ceramic	**
Ozel [8]	LCFCS	Uncoated WC	100
Xie et al [9]	AISI 1045	Uncoated WC	10
Miguelez et al [10]	42CrMo4	Uncoated WC	**
Coelho et al [11]	AISI 4340	PCBN	500
Arrazola et al [12]	AISI 4140	ISO P10 carbide	100000

***Value not reported. Perfect contact was assumed between tool and workpiece.*

cutting speed. Their assumption was based on experimental results for temperature and chip surface in the secondary deformation zone. Marusich and Ortiz [7] used the first law of thermodynamics to account for thermal effects produced during the cutting process. The heat generated at the sliding contact was considered to be a function of the difference in the velocity across the contact. This was divided proportionately between the tool and the chip based on their thermal conductivity, density and heat capacity values. Ozel [8] used a value of 100 kW/m^2 ^{o}C (4.89 BTU/sec/ft^2/^{o}F) as interface heat transfer coefficient for studying the effect of different friction models on the output of orthogonal machining process. Xie et al. [9] simulated 2D tool wear in turning of AISI 1045 steel with an uncoated tungsten carbide tool at a cutting speed of 300 m/min. Their FE model used a value of 10 kW/m^2 ^{o}C (0.49 BTU/sec/ft^2/^{o}F) to define the gap conductance at the tool-chip interface. Miguelez et al. [10] simulated orthogonal metal cutting process by using two different numerical approaches, i.e. Lagrangian and Arbitrary Lagrangian Eulerian, with different chip separation criteria. Here, the relation defining the heat flux crossing the tool-chip interface was directly related to interface gap conductance. The value of gap conductance was again assumed to be very high for perfect heat transfer between the tool and the chip. Coelho et al. [11] simulated orthogonal metal cutting process using Arbitrary Lagrangian Eulerian approach for AISI 4340 steel as workpiece and PCBN as cutting tool using finishing cutting parameters. A gap conductance value of 500 kW/m^2 ^{o}C (24.5 BTU/sec/ft^2/^{o}F) was used considering perfect heat transfer. Arrazola et al. [12] simulated the orthogonal metal cutting process, for the study of serrated chip formation during simulation of metal cutting process using Arbitrary Lagrangian Eulerian approach. They analysed the sensitivity of serrated chip prediction to the numerical and cutting parameters using AISI 4140 steel as workpiece and uncoated ISO P10 grade carbide as cutting tool. A gap conductance value of 10^5 kW/m^2 ^{o}C (4.89 BTU/sec/ft^2/^{o}F) was used considering heat transfer with perfect thermal contact. **Table 1** summarizes the values of the interface heat transfer coefficients used for the simulation of metal machining process.

3. METHODS USED PREVIOUSLY FOR THE ESTIMATION OF INTERFACE HEAT TRANSFER COEFFICIENT

Many different approaches have been used to estimate interface heat transfer coefficient. However, most of the previous work focused on hot and cold forming processes rather than machining. For these (forming) processes, analytical, experimental and numerical approaches were used to define and estimate heat transfer between solids under sliding contact. Most of the analytical studies estimated the contact temperature by considering two semi infinite solids under steady-state conditions and assuming a band, circular or elliptic shaped contact, with applications in strip rolling [13-16]. Bos and Moes [17] used asymptotic solutions for circular and semi-elliptic band contact to analyse heat partitioning problem by matching surface temperatures. Their solutions covered a wide range of Peclet numbers. Bauzin and Laraqi [18] used the least square method to estimate the heat generated, thermal contact conductance and heat partition coefficient simultaneously.

The experimental work has mainly focused on the determination of heat partition and thermal contact conductance. Berry and Barber [19] developed a symmetric cylinder on cylinder experimental setup to study the division of frictional heat in sliding contact. They concluded that oxide films have an appreciable effect on microscopic thermal resistance. Lestyan et al. [20] developed a test rig to perform dry sliding of alumina-steel pair to analyse contact and temperatures developed in the

contact region. Some experimental studies, for determining the thermal contact conductance, were conducted using devices which contained two tools or two tools with a workpiece sandwiched between them [21-24]. These experiments were followed by an assessment of the interface heat transfer coefficient whilst the specimen deformed plastically. Another method was based on the solution of an inverse problem; a sequential inverse method was used to determine the thermal contact conductance in metal forming processes [25]. A further method was based on matching the experimentally measured temperature with analytical and/or numerical solutions for various values of '*h*'. The interface heat transfer coefficient was taken to be the value which provided the best match between simulation and experimental results [23-24,26].

4. EFFECT OF OPERATING PARAMETERS ON '*H*' VALUE IN FORGING PROCESSES

As mentioned earlier, the interface heat transfer coefficient is influenced by several operating parameters such as pressure, macro and micro geometries of the contacting surfaces and temperature. In this section, the effects of these operating parameters on the interface heat transfer coefficient are discussed.

4.1 Effect of Pressure

During the forging process, the pressure applied by closing the die largely influences the interface heat transfer coefficient. Semiatin et al. [21] reported an experimental and analytical technique for the determination of interface heat transfer coefficient for non-isothermal bulk forming process. Two instrumented dies were heated to different temperatures and brought together under varying pressure levels. A one dimensional analysis and a finite difference model were used in the evaluation of interface heat transfer coefficient. They concluded that in the absence of deformation, the heat transfer coefficient increases with increasing interface pressure. Above a threshold pressure, the interface heat transfer coefficient becomes insensitive to the forging pressure. Similar results were reported by Lambert et al. [27] and Lambert and Fletcher [28]. They produced design graphs for the thermal contact conductance for three major aerospace alloys, with pressure up to 100 MPa (7.25 tons/in^2) and temperature of 300 ^{o}K (80 ^{o}F). Hu et al. [29] also reported a similar trend of increase in heat transfer coefficient with increasing interface pressure, for the forging of Ti6Al4V alloy. The temperature and pressure taken in their study were 920 ^{o}C (1688 ^{o}F) and 500 MPa (36.25 tons/in^2), respectively.

4.2 Effect of Temperature

Malinowski et al. [22] studied heat transfer coefficient as a function of temperature and pressure. They used temperature measurement in two dies in contact and employed FE method to determine the interface heat transfer coefficient. They developed an empirical relationship giving interface heat transfer coefficient as a function of time, temperature and interfacial pressure. However, they neglected the heat generation within the workpiece. They concluded that interface heat transfer coefficient was not as strongly dependent on temperature as on pressure.

4.3 Effect of Interface Friction

Burte et al. [24] studied the coupling between heat transfer coefficient and friction during hot forging process. They analysed the data from ring compression tests combined with generation of heat transfer coefficient and friction shear factor calibration curves derived from FE simulations. They reported that the effect of friction shear factor on heat transfer coefficient was small. Their simulation results and corroborating experimental observations led to the conjecture that heat transfer and friction may be decoupled in the analysis of metal working process for similar geometry and processing conditions.

4.4 Effect of Deformation Speed

Semiatin et al. [21] deduced from a ring compression test, involving both deformation and heat transfer, that the heat transfer coefficient increased with deformation rate. Similar trend was also reported by Hu et al. [29], with strain rates of 0.125 s^{-1} and 1.0 s^{-1} and with higher values of pressure and temperature as compared to ones used by Semiatin et al. [21]. This can be explained by the fact that at high deformation rates, most of heat transfer occurs simultaneously with the process which tends to smooth interface asperities. On the contrary at low deformation rates, heat transfer occurs prior to large deformation.

4.5 Effect of Surface Roughness

Lambert and Fletcher [28] studied the effect of a non-flat, rough and metallic coated surface on thermal contact conductance. They concluded that the interface heat transfer coefficient increased with increasing roughness of contacting surfaces. Rough surfaces add more resistance to the transfer of heat. Similarly in the case of lubricants and coatings, applied to the interface during forging process to reduce interfacial friction, also adds to the resistance to heat transfer between contacting surfaces, thereby resulting in a reduction in interface heat transfer coefficient.

5. COMPARISON BETWEEN MACHINING AND FORGING PROCESS: OPERATING CHARACTERISTICS

Based on the discussion presented earlier, there are some contrasting factors related to the nature of bulk forming and machining. In the case of hot bulk forming process, the interface heat transfer coefficient is influenced by rate of deformation encountered during the process. The maximum strain rates involved in forging processes are of the order of 10^3 s^{-1} [30] and are relatively low as compared to the machining process. The deformation rates involved during the machining processes, on the other hand, are very high typically of the order of 10^6 s^{-1} [31]. Similarly the difference in temperatures involved in these processes is very high. Kalpakjian [30] reported that homologous temperature (ratio of operating temperature to the melt temperature) for forging processes ranges between 16%-70%, whereas for machining process it can go up to 90%, i.e. closer to the melt temperature and higher as compared to forging processes.

The contact area is also a critical issue in this comparison, as it provides a passage for heat transfer between mating surfaces. In the case of metal machining, the contact area between the tool and the chip is small and does not vary substantially during the machining process. In machining of AISI 1045 steel with uncoated cemented carbide, the contact area decreases with increasing cutting speed for cutting speed up to 900 m/min (2953 feet/min) [32]. However, in the case of metal forging (considering the case of upset forging), the contact area increases substantially with increasing percentage reduction in height during the forming process. Also, the nature of contact in the two processes under consideration is different. In the case of forging, mating components remains in contact during the whole process whereas, in the case of machining, fresh workpiece material comes in contact continuously with the tool rake face. For the latter case, it is necessary to develop an experimental setup for the determination of interface heat transfer coefficient suitable for the machining process.

6. RUBBING EXPERIMENTS

An experimental setup adapted from that proposed by Lancaster [33] and Olsson [34], for the study of wear was used in this case to study the heat transfer problem. Rubbing tests were performed, where the end surface of a cylindrical pin made of tool material was pressed against the end surface of a rotating workpiece. For these tests, a pin of 2.5 mm (0.1 in.) diameter and 15 mm (0.6 in) length was made of cemented tungsten carbide (same grade as ISO P10- P20 cutting tool). The end surface of the pin was ground to a negative relief angle (approximately 5°- 10°) so as to avoid chip formation. The mass of the pin was measured using a precision electronic balance to calculate the amount of weight loss during the rubbing process. The pin was assembled on the tool holder in order to regulate its radial position compared to the thickness of the cylindrical workpiece. The tool holder was then mounted on a Kistler 3 component piezoelectric dynamometer to measure forces. An AISI 1045 workpiece of a hollow cylindrical shape with a wall thickness of 2.5 mm (0.1 in.) was used. The rubbing experiments were performed at the rubbing speeds of 56, 139, 195, 279, 391, 441, 558 and 776 m/min (2.5 feet/min), on a lathe machine equipped with an infrared thermal imaging camera and a force dynamometer. The rubbing time was set to one minute for all rotational speeds in order to achieve a steady state temperature in the pin and the experiments were repeated three times. The experimental setup is shown in **Figures 1**-**2**. The temperatures were measured using an infrared thermal imager FLIR ThermalCAM_ SC3000. This system is a long-wave and self-cooling analysis system with a cool down time of less than six minutes. The accompanied software package allows detailed analysis of highly dynamic objects and events typically found in metal machining applications. The thermal imaging camera has a temperature range of 20 ^{o}C (68^{o}F) to 2000 ^{o}C (3632 ^{o}F) with an accuracy of ±2 ^{o}C (36 ^{o}F) for measurement range above 150 ^{o}C (302 ^{o}F) . This camera can capture and store thermal images and data at high rates (up to 750 Hz for PAL and 900 Hz for NTSC format) with the ThermaCAM Researcher^{TM} 2.8 package. Complete technical specifications of the thermal imaging system are given in **Table 2**. **Figure 2** shows the position of thermal imaging camera in the experimental setup. The camera was positioned at a distance of 45 cm (18 in.) from the pin. The

stored images were recalled and analysed by using the available software. When placed on the image the cursor gave the temperature value at the required points. For the rubbing time specified, the pin acquired a uniform temperature in the portion extended from the holder. The real temperature of an object depends strongly on the emissivity of the material, which is of particular concern when a thermal imaging camera is used. An accurate calibration of the thermographic system was carried out to find the emissivity value of the rubbing pin material (uncoated cemented carbide, ISO P20 grade). Samples were heated to temperatures ranging from 100 to 900 ^{o}C (212 to 1652 ^{o}F) in an oven. A thermocouple-infrared pyrometer arrangement was used to read the temperature of the pin, and the emissivity adjusted until the temperature reading of the pyrometer matched a thermocouple reading. The average thermal emissivity of the uncoated cemented carbide pin was found to be 0.55 at 700 ^{o}C (1292 ^{o}F) .

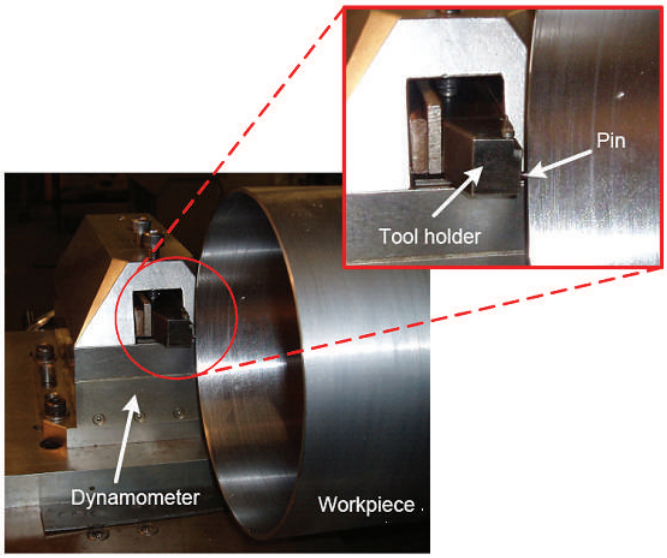

Figure 1. Experimental setup for the pin rubbing tests

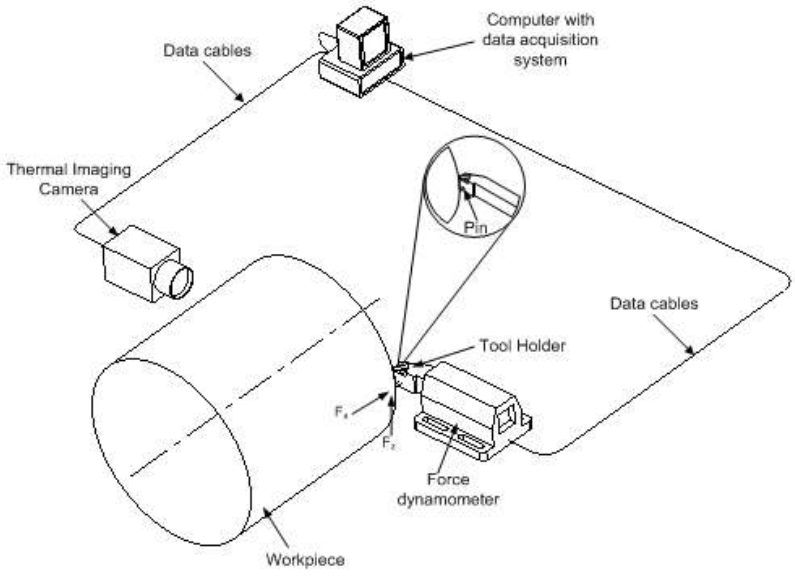

Figure 2. Schematic representation of the experimental setup for the pin rubbing test (showing position of thermal imaging camera)

Table 2. Technical specifications of FLIR system IR thermal imaging camera

IR detector	Quantum well IR photodetector (QWIP)
Spectral range	8-9 μm
Image frequency	50/60 Hz non-interlaced (standard), up to 750/900 Hz (optional and with Researcher HS option)
Thermal sensitivity	20 mK at 30 °C
Temperature range	-20 °C to +2000°C
Accuracy	±1°C (for measurement ranges up to +150 °C) ±2°C (for measurement ranges above +150 °C)
Spatial resolution	1.1 mrad
Pixel per image	320 x 240
Zoom factor	4 x
File format	14-bit radiometric IR digital image (*.IMG) 8-bit standard bitmap(*.BMP)

7. EXPERIMENTAL RESULTS AND DISCUSSIONS

The experimental results are presented in **Figures 3, 5** and **7**. Each data point on these graphs was calculated from measurement of three rubbing tests, shown with corresponding variation in data. **Figure 3** shows the variation of coefficient of friction with rubbing speed. This was calculated from the forces measured during the rubbing process. It shows an overall decreasing trend with increasing rotating speed, similar to the results of other cutting experiments . However, the numerical values of the friction coefficient obtained from these rubbing tests are lower as compared to the previously reported values of cutting experiments for a similar range of speeds . This could be explained by the absence of any sticking in the rubbing tests as compared to the cutting experiments. **Figure 4** shows the variation of maximum temperature measured at a specified location on the pin, with respect to time. Initially there are a few spikes of high temperature (due to the chip formation) but soon afterwards the temperature becomes steady. **Figure 5** shows the variation of pin temperature with rubbing speed. The pin temperature rises sharply in the speed range of 195 to 558 m/min but then stabilizes after that speed in the temperature range of 700 °C to 900 °C (1292 to 1652 °F) . This can be explained in the context of the variation of thermal conductivity of uncoated cemented tungsten carbide. Child et al. reported that the thermal conductivity of ISO P grade uncoated cemented tungsten carbide decreases with increasing temperature (**Figure 6**). This can account for the flatter slope of pin temperature curve at high speeds. The variation of pin wear with rubbing speed is shown in **Figure 7**. Initially the pin material loss is low up to a rubbing speed of 279 m/min (915 ft/min) but it rises sharply at a rubbing speed of 391 m/min (1283 ft/min). It then drops slightly at a rubbing speed of 441 m/min (1447 ft/min) but increases again at a steady rate. It should be noted that the variation in pin temperature and pin weight loss with rubbing speed follow a similar trend. **Figure 8** shows that pressure is approximately constant for all the rubbing speeds, except for the lowest speed. It is evident from the results presented in **Figure 3, 5** and **7**, that there is a marked transition in their behaviour. There are three regions which can be identified for all three variables; Region–I, for speed less than 200 m/min (656 ft/min), region-II, for speed greater than 200 m/min (656 ft/min) and less than 600 m/min (1969 ft/min), and region-III, for speeds greater than 600 m/min (1969 ft/min). For rubbing speed less than and equal to 200 m/min (656 ft/min) (region-I), the loss of pin mass is negligible. For rubbing speed interval of 200-600 m/min (656-1969 ft/min), the loss of pin mass is very high. Similarly temperature rises sharply in regions I and II but stabilises in region III. Correspondingly the coefficient of friction decreases in these two regions i.e. in regions I and II and stabilises in region III. In the next section a FE model of the pin rubbing setup will be discussed. The scheme followed is to vary the interface gap conductance to match the experimental pin temperature.

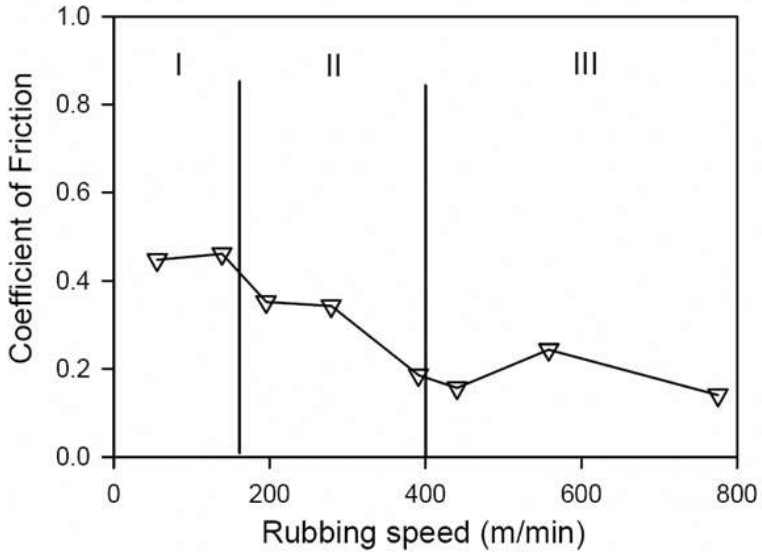

Figure 3. Variation of coefficient of friction with cutting speed

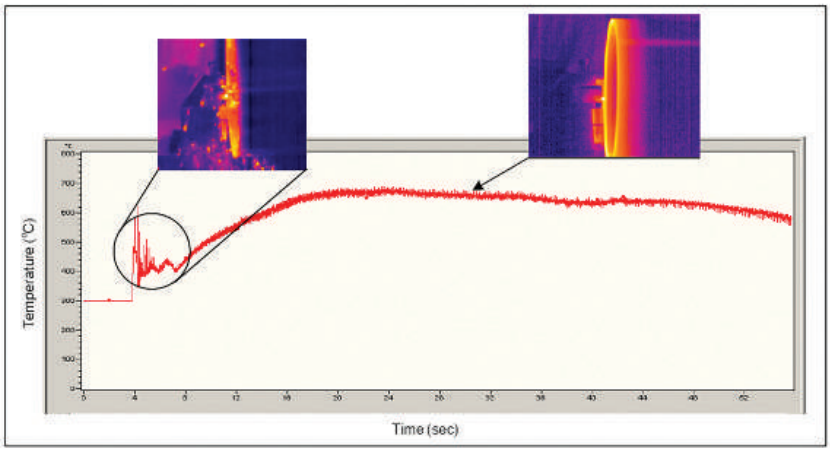

Figure 4. Maximum pin temperature measured during the rubbing process, using the thermal imaging camera

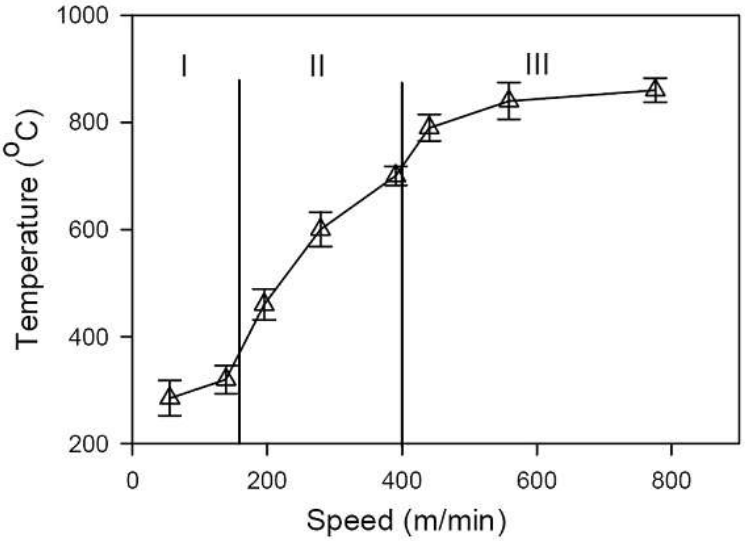

Figure 5. Variation of pin temperature with cutting speed

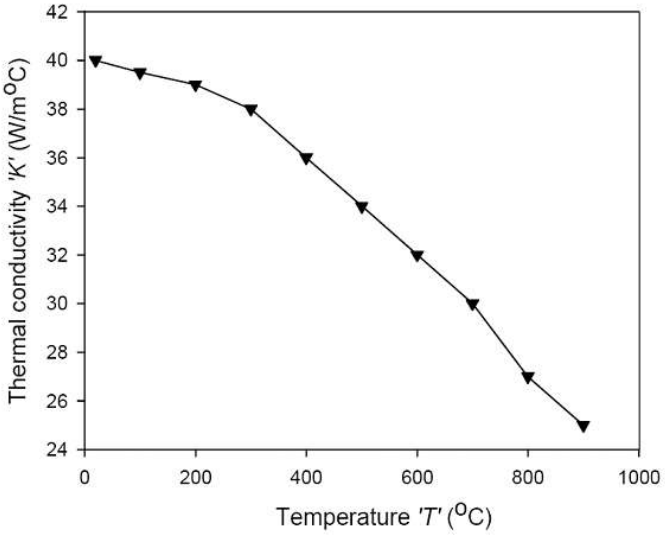

Figure 6. Variation of thermal conductivity with temperature for P20 carbide [36

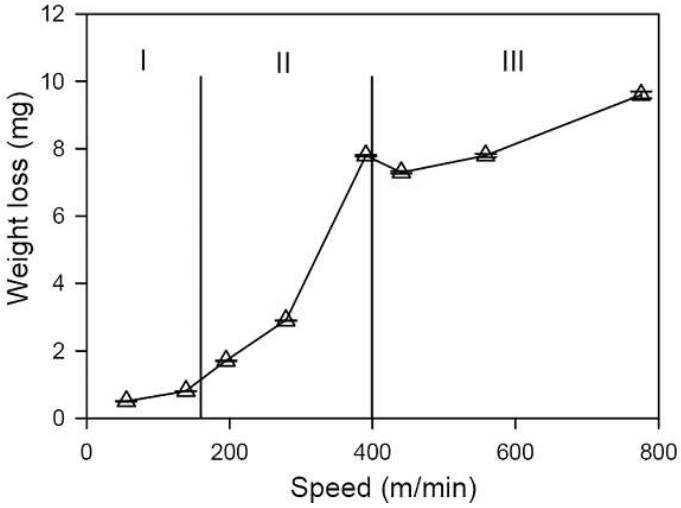

Figure 7. Variation of weight loss of pin with cutting speed

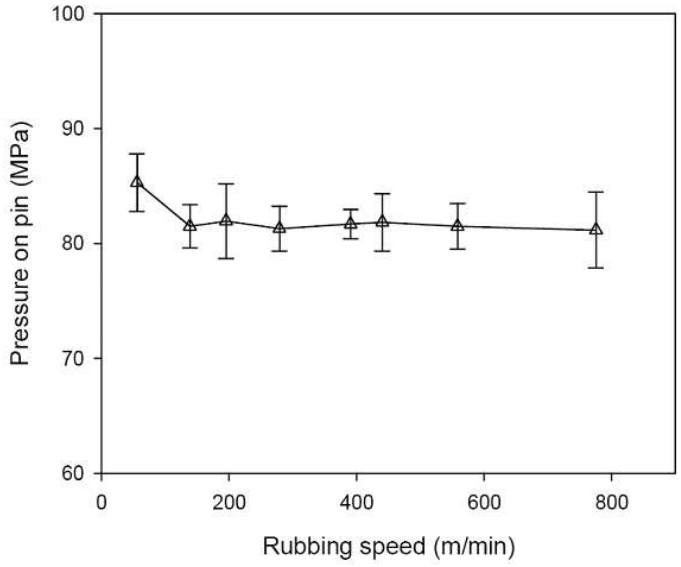

Figure 8. Variation of pressure applied on the pin at different rubbing speeds

8. FE MODELLING

In order to numerically simulate the rubbing process, a commercial FE package ABAQUS/Explicit was used. An FE model was developed and the simulations were run with conditions similar to the experiments. As the problem involved a number of strongly interacting mechanical and thermal processes like friction, temperature and wear, a coupled thermo-mechanical model was developed. The heat produced by friction (mechanical work) acts as a source for the thermal problem. The work presented here is based on the rubbing process only, i.e. wear is neglected. This is justifiable because the volume of material removed (in milligrams) from the pin during rubbing process was very low compared to the advanced wear processes involved in real machining. The FE model used for simulating the rubbing process is shown in **Figure 9**. In this model, the carbide pin was held stationary, while the AISI 1045 steel workpiece revolves with a rubbing speed ranging from 56 to 776 m/min (184 to 2546 ft/min). A graded mesh was used for both the pin and workpiece, with higher mesh density in the interface zone. With reference to **Figure 9**, the boundary conditions used for the model are defined as follows: the contact surfaces of the pin and the workpiece were assumed to be smooth and in perfect contact. The contact between the pin and workpiece was evaluated by using an optical microscope to examine the pin face. The wear marking on the pin showed full contact. The exterior boundaries are exposed to still air except the contacting regions of the pin and the workpiece. For exterior regions, the convective heat transfer coefficient is assumed to be h_∞ = 0.02 kW/m^2 ^{o}C (9.7 x 10^{-4} BTU/sec/ft^2/^{o}F) . Any heat loss due to radiation is neglected. The whole model was set at room temperature. The experimental values of coefficient of friction (shown in **Figure 3**) are used at the interface of the pin and the counter material for each rubbing speed. The material properties used for the pin and the workpiece materials are listed in **Table 3**. In the application of contact formulation for FE model, the carbide pin is taken as the 'slave' and the AISI 1045 steel workpiece as the 'master'. Heat partition is an important issue in sliding contact of two bodies for which several approaches have been followed by different researchers . For FE model developed for this study, the heat partition ratio at the interface between the pin and the workpiece is given mathematically by Eq. 2.

$$\frac{H_1}{H_2} = \frac{\sqrt{\rho_1 C_1 K_1}}{\sqrt{\rho_2 C_2 K_2}} \qquad (2)$$

where H is the heat partition, is the density (kg/m^3), K is the thermal conductivity (W/m^2 ^{o}C) and C is the specific heat capacity (J/m^2 ^{o}C). Subscripts 1 and 2 represent the pin and workpiece materials respectively. Temperature dependent data, given in **Table 3**, was used to evaluate Eq. 2.

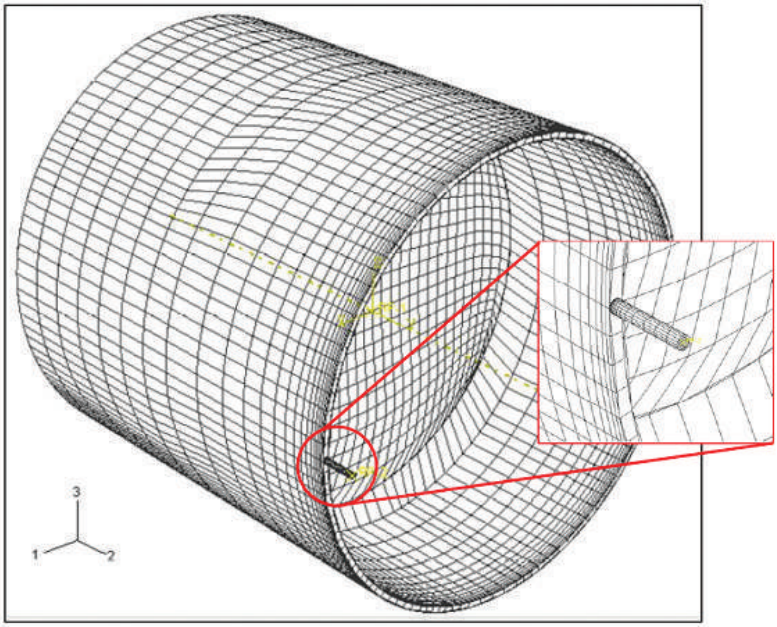

Figure 9. FE model of the rubbing process

Table 3. Material properties of Pin and counter material [37]

Thermal/ mechanical properties	**Tool : Uncoated cemented carbide***	Poisson's ratio		0.3											
		Thermal Expansion	^oC	20-800											
			$^oC\ ^{-1}(x10^{-06})$	6.3											
		Heat Capacity	^oC	240	450	640	695								
			$N.mm^{-2}.^oC^{-1}$	3.66	3.8	4.31	5.1								
		Modulus of elasticity	^oC	20	200	300	500	700							
			GPa	520	509	494	487	487							
		Thermal Conductivity	^oC	20	100	200	300	400	500	600	700	800	900		
			$W.m^{-1}.^oC^{-1}$	40	39.5	39	38	36	34	32	30	27	25		
	Workpiece: AISI 1045	Poisson's ratio		0.3											
		Thermal Expansion	^oC	20	200	400	600								
			GPa	215	210	165	160								
		Heat Capacity	^oC	100	200	300	400	500	600	700					
			$^oC\ ^{-1}(x10^{-05})$	1.12	1.19	1.27	1.35	1.41	1.45	1.46					
		Modulus of elasticity	^oC	25	125	325	525	725	825	875	925	975			
			$N.mm^{-2}.^oC^{-1}$	3.66	3.8	4.31	5.1	8.76	8.27	7.48	6.04	5.64			
		Thermal Conductivity	^oC	25	100	300	500	700	800	900	950	1000	1050	1100	1150
			$W.m^{-1}.^oC^{-1}$	45	42.5	38	34.5	29	28	24	23	23	24	26	27

* Room temperature properties are provided by Sandvik Coromant. For temperature dependent properties, data from [36] is followed.

The interface heat transfer coefficient between the pin and the workpiece is defined in the FE model by gap conductance. This parameter controls the amount of heat flowing through the interface. The strategy used here was to vary the value of gap conductance in the simulation and match the simulated temperatures on the pin with experimental values at the same location. For the matched temperatures, the gap conductance value used in the simulation defined the interface heat transfer coefficient. During the rubbing experiments, only a small length of the pin protruded from the tool holder in order to avoid any excessive pin deflection or breakage. Due to this short protruded length of the pin, the measured temperature of the pin was almost uniform.

9. NUMERICAL RESULTS

A series of simulations for all the rubbing speeds ranging from 56 to 776 m/min were carried out. The interface heat transfer coefficient values for these speeds, following the procedure outlined in the previous section, are shown in **Figure 10**. These results show that the value of interface heat transfer coefficient is initially high (300 $kW/m^2\ ^oC$ (14.67 $BTU/sec/ft^2/^oF$) for a low rubbing speed of 56 m/min (184 ft/min). The value then reduces to 100 $kW/m^2\ ^oC$ (4.89 $BTU/sec/ft^2/^oF$) at 139 m/min (456 ft/min) and remains constant until the rubbing speed of 279 m/min (915 ft/min). After that, it increases to a value of 150 $kW/m^2\ ^oC$ (7.34 $BTU/sec/ft^2/^oF$) for the rubbing speed of 441 m/min (1447 ft/min) and again decreases to a value of 100 $kW/m^2\ ^oC$ (4.89 $BTU/sec/ft^2/^oF$) at 776 m/min (2546 ft/min). By examining the pin temperatures for this speed range (**Figure 5**), the pin temperature rises steadily before stabilizing for high rubbing speeds (>558 m/min (1831 ft/min)). The pin wear rate shows a direct dependence on the pin temperature (**Figure 5**). As shown in **Figure 8**, the pressure corresponding to the load applied on the pin approximately remains constant except for the very low speed. In this context, by comparing **Figure 5** and **Figure 10**, it is observed that the interface heat transfer coefficient initially shows a decreasing trend with temperature (for the two lowest rubbing speeds) and afterwards it becomes constant for high rubbing speeds. Thus the interface heat transfer coefficient shows a dependence on the temperature for low rubbing speeds (**Figure 11**). For the forging methods, the temperature of both the workpiece and the die are varied for the estimation of interface heat transfer coefficient. Also, heat generated during bulk forming is involved in the process. For the rubbing process on the other hand, both the pin and the workpiece are at surrounding temperature and the source of heat generation is rubbing and sliding only. As mentioned earlier, Malinowski reported that the interface heat transfer coefficient is strongly

dependent on die pressure and not on die temperature. Here, the interface heat transfer coefficient shows a modest dependence on temperature attained during the process. It may be noted that the slight increase in the interface heat transfer coefficient value is for the rubbing speed range of 391–558 m/min (1283-1831 ft/min) which falls under the conventional to high speed machining transition range for AISI 1045 steel . It is also important to note that all the estimated values of interface heat transfer coefficient '*h*' vary between 100 to 300 kW/m^{2}ºC (4.89 to 14.68 BTU/sec/ft^2/ºF). These values fall within the range of assumed values used previously for the simulation of metal machining process (10-500 kW/m^2 ºC) (0.49-24.46 BTU/sec/ft^2/ºF). However, the range is narrower than before. Another important point is that wear of the pin material is not considered in the modelling of rubbing process. This was justifiable because only minute pin wear was recorded (**Figure 7**). Significant pin wear may affect the interface heat transfer coefficient value. However, FE modelling of wear mechanisms is a challenging and ongoing task.

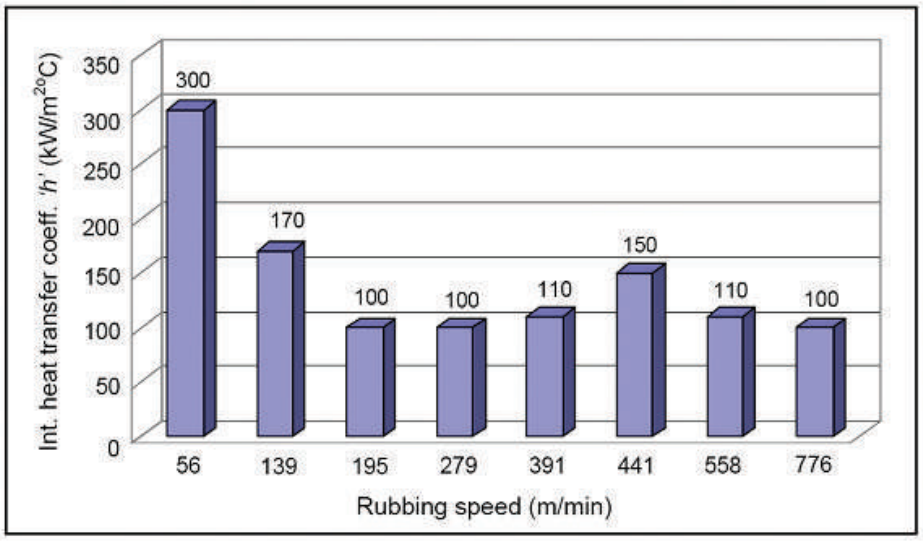

Figure 10. Variation of the interface heat transfer heat coefficient with rubbing speed

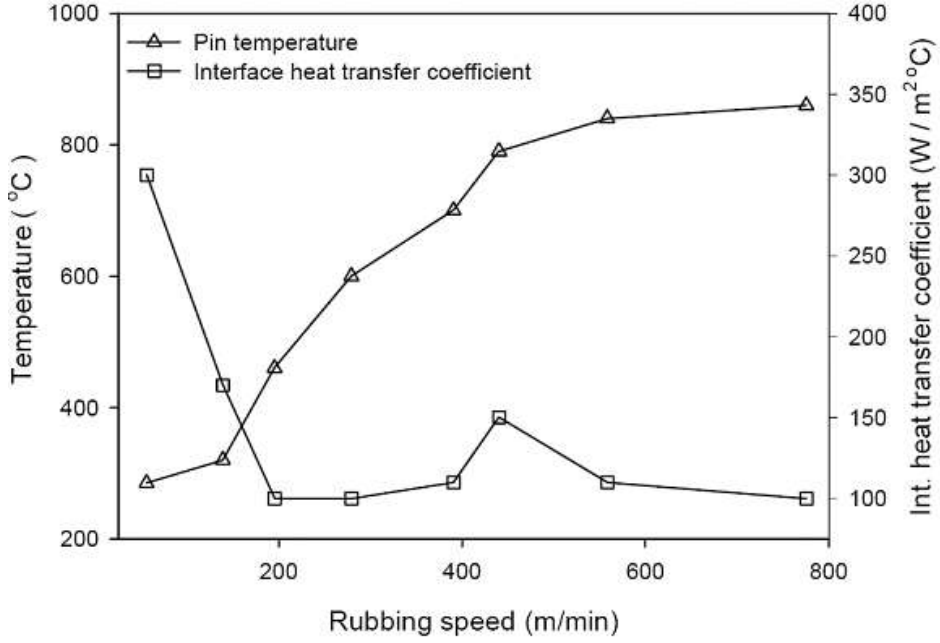

Figure 11. Variation of the pin temperature and interface heat transfer coefficient with rubbing speed

10. CONCLUSIONS

Based on the findings from experimental and modelling results, following conclusions can be drawn:

- Interface heat transfer coefficient is an important parameter which quantifies the amount of heat transferred to the cutting tool in the FE modelling of mechanical machining processes. The resulting temperature distribution in the cutting tool is, in turn important for the modelling of tool wear processes. The present practice is to use interface heat transfer coefficient values estimated from metal forging process, based on the assumption of perfect contact.
- Based on the operating range of strain, strain rate and temperature, the nature of contact in forging and machining processes are dissimilar. An experimental procedure close to the machining process should be used for the estimation of interface heat transfer coefficient.
- A new method based on rubbing of a carbide pin of material similar to the cutting tool with AISI1045 steel as counter material was employed. In addition, an FE model of the rubbing process was developed for the estimation of interface heat transfer coefficient for a wide range of rubbing speeds.
- Results show that the estimated interface heat transfer coefficient decreases at low rubbing speeds and then becomes approximately constant for high rubbing speeds. At these low rubbing speeds, the estimated values show a dependence on temperature.
- All the estimated values of interface heat transfer coefficient '*h*' lie between 100–300 $kW/m^2\,^oC$ (4.89-14.68 $BTU/sec/ft^2/^oF$). A majority of cutting speeds can be modelled by using *h* value equal to 100 $kW/m^2\,^oC$ (4.89 $BTU/sec/ft^2/^oF$). Results suggest that assuming '*h*' values lower than 100 $kW/m^2\,^oC$ (4.89 $BTU/sec/ft^2/^oF$) or greater than 300 $kW/m^2\,^oC$ (14.68 $BTU/sec/ft^2/^oF$) would lead to errors in the estimation of thermal fields and chip morphology. Values of 10 $kW/m^2\,^oC$ (4.89 $BTU/sec/ft^2/^oF$), 500 and 100,000 $kW/m^2\,^oC$ (24.46 and 4892 $BTU/sec/ft^2/^oF$) have been assumed by some previous researchers without proper justification.

REFERENCES

1] O'Sullivan D, Cotterell M. Temperature Measurement in Single Point Turning. J Materials Processing Technology 2001;118:301-308.

[2] Madhusudana CV. Thermal Contact Conductance. Springer, Berlin, 1996,. p. 1-23.

[3] Yen Y-C, Jain A, Altan T. A Finite Element Analysis Of Orthogonal Machining Using Different Tool Edge Geometries. J Materials Processing Technology 2004;146:72-81.

[4] Yen Y-C, Sohner J, Lilly B, Altan T. Estimation of Tool Wear In Orthogonal Cutting Using Finite Element Analysis. J Materials Processing Technology 2004;146:82-91.

[5] Yen Y-C, Jain A, Chigurupati P, Wu W-T, Altan T. Computer Simulation Of Orthogonal Metal Cutting Using A Tool With Multiple Coatings. Machining Science and Technology 2004;8(2):305-326.

[6] Klocke F, Raedt H-W, Hoppe S. 2D-FEM Simulation of the Orthogonal High Speed Cutting Process. Machining Science and Technology 2001;5(3):323–340.

[7] Marusich TD, Ortiz M. Modelling and Simulation of High-Speed Machining. J Numerical Methods in Engineering 1995;38:3675 -3694.

[8] Ozel T. The Influence Of Friction Models On Finite Element Simulations Of Machining. J Machine Tools and Manufacture 2006;46(6):518-530.

[9] Xie L-J, Schmidt J, Schmidt C,Biesinger F. 2D FEM Estimate Of Tool Wear In Turning Operation. Wear 2005;258:1479–1490.

[10] Miguelez H, Zaera R, Rusinek A, Moufki A, Molinari A. Numerical Modelling Of Orthogonal Cutting: Influence Of Cutting Conditions And Separation Criterion. Journal De Physique 2006;134:417-422.

[11] Coelho RT, Ng E-G, Elbestawi MA. Tool Wear When Turning AISI 4340 with Coated PCBN Tools Using Finishing Cutting Conditions. J Machine Tools & Manufacture 2007;47:263-272.

[12] Arrazola PJ, Villar A, Ugarte D, Marya S. Serrated Chip Prediction In Finite Element Modelling Of The Chip Formation Process. Machining Science and Technology 2007;11(3):367-390.

[13] Yuen WYD. Heat Conduction In Sliding Solids. J Heat and Mass Transfer 1988;31(3):637-646.

[14] Cameron A, Gordon AN, Symm GT. Contact Temperatures in Rolling/Sliding Surfaces. Proceedings of the Royal Society of London. Series A, Mathematical and Physical Sciences 1965;286(1404):45-61.

[15] Symm GT. Surface Temperature Of Two Rubbing Bodies. J Mechanics and Applied Mathematics, 1967; 20(3): 381-391.

[16] Barber JR. The conduction of heat from sliding solids. J Heat and Mass Transfer 1970;13:857-869.

[17] Bos J, Moes H. Frictional Heating Of Tribological Contacts. Transaction of ASME. J Tribology 1995;117:171-177.

[18] Bauzin J-G, Laraqi N. Simultaneous Estimation Of Frictional Heat Flux And Two Thermal Contact Parameters For Sliding Contact. Numerical heat transfer, Part-A, 2004;45:313-328.

[19] Berry GA, Barber JR. The Division Of Frictional Heat- A Guide To The Nature Of Sliding Contact. Transaction of ASME. J Tribology 1984;106:405-417.

[20] Lestyan Z, Varadi K, Albers A. Contact and Thermal Analysis Of An Alumina-Steel Dry Sliding Friction Pair Conisdering The Surface Roughness. J Machine Tools & Manufacture 2007;40:982-994.

[21] Semiatin SL, Collings EW, Wood VE, Altan T. Determination of the Interface Heat Transfer Coefficient For Non Isothermal Bulk Forming Process. Transactions of the ASME. J Engineering for Industry 1987;109:49-57.

[22] Malinowski Z, Lenard JG, Davies ME. A Study Of The Heat-Transfer Coefficient As A Function Of Temperature And Pressure. J Materials Processing Technology 1994;41:125-142.

[23] Nshama W, Jeswiet J. Evaluation of Temperature And Heat Transfer Conditions At The Metal Forming Interfaces. Annals of CIRP 1995;44(1):201-205.

[24] Burte PR, Yong-Tack I, Altan T, Semiatin SL. Measurements and Analysis Of The Heat Transfer And Friction During Hot Forging. Transactions of the ASME. J Engineering for Industry 1990;112:332-339.

[25] Goizet V, Bourouga B, Bardon JP. Experimental Study Of The Thermal Boundary Conditions At The Workpiece–Die Interface During Hot Forging. In *11th IHTC*. Kyongju, Korea: 1998. Taylor and Francis, London.

[26] Dadras P,Wells WR. Heat Transfer Aspects Of Non-Isothermal Axisymmetric Upset Forging. Transactions of the ASME. J Engineering for Industry 1984;106:187-195.

[27] Lambert MA, Mirmira SR, Fletcher LS. Design Graphs For Thermal Contact Conductance Of Similar And Dissimilar Light Alloys. J Thermophysics and Heat Transfer 2006;20(4):809-816.

[28] Lambert MA, Fletcher LS. Thermal Contact Conductance Of Non Flat, Rough, Metallic Coated Metals. Transactions of the ASME. J Heat Transfer 2002;124:405-412.

[29] Hu ZM, Brooks JW, Dean TA. The Interfacial Heat Transfer Coefficient In Hot Die Forging Of Titanium Alloy. Proc. IMechE Part C: J. Mech. Engg. Sci. 1998;212(6):485-496.

[30] Kalpakjian S. Manufacturing processes for engineering materials. Addison-Wesley/Longman, Menlo park, 3rd ed., 1997. p. 43-102.

[31] Childs THC, Rowe GW. Physics in Metal Cutting. Reports on Progress in Physics 1973;36(3):223-288.

[32] Iqbal SA, Mativenga PT, Sheikh MA. Characterization of the Machining of AISI 1045 Steel over a Wide Range of Cutting Speeds-Part 1: Investigation of Contact Phenomena. Proc. IMechE Part B: J. Engineering Manufacture 2007;221(5):909-916.

[33] Lancaster J. The formation Of Surface Films At The Transition Between Mild And Severe Metallic Wear. Proceedings of Royal Society A 1963;273:466-483.

[34] Olsson M, Soderberg S, Jacobson S, Hogmark S. Simulation of Cutting Tool Wear By A Modified Pin-On-Disc Test. J Machine Tools and Manufacture 1989;29(3):377-390.

[35] Devillez A, Lesko S, Mozerc W. Cutting Tool Crater Wear Measurement With White Light Interferometry. Wear 2004;256(1-2):56-65.

[36] Childs THC, Maekawa K, Obikawa T, Yamane Y. Metal machining: Theory and application. London: Arnold, London, 2000.

[37] Abukhshim NA, Mativenga PT, Sheikh MA. Investigation of Heat Partition In High Speed Turning Of High Strength Alloy Steel. J Machine Tools and Manufacture 2005;45(15):1687-1695.

[38] Gecim B, Winer WO. Transient Temperatures In The Vicinity Of An Asperity Contact. Transactions of the ASME. J Tribology 1985;107:333-342.

[39] Grzesik W, Nieslony P. A Computational Approach To Evaluate Temperature And Heat Partition In Machining With Multilayer Coated Tools. J Machine Tools and Manufacture 2003;43:1311-1317.

[40] Schulz H, Moriwaki T. High Speed Machining. Annals of CIRP 1992;41(2):637-644.

NED UNIVERSITY
JOURNAL OF RESEARCH

GUIDELINES TO AUTHORS

The NED University Journal of Research policy describes the principles for all publications. This document elaborates the requirements for submission of manuscript for the Journal. Please submit your manuscript as a **MS Word** file attachment to the Editor at NED-Journal@neduet.edu.pk.

General

The manuscript must report and original and unpublished work. It must be based on significant factual records and be significant in the findings. The suitability of a manuscript for publication will be evaluated by the reviewers who will provide justification for publication.

The manuscript should be clean without showing changes, corrections or deleted material marked on the manuscript. It is the responsibility of authors to check symbols, abbreviations, units and technical terms for accuracy, consistency and legibility. **Footnote and endnotes are not permitted.** All the necessary information should be incorporated within the text of the paper. Gender specific words (such as he, she, etc) should be avoided. Use of the third person is encouraged. Both SI and US Customary units should be used throughout the paper including figures and tables. Provide the conversion factors for the units used in the table or figure under the table or figure if space prevents use of secondary units in the same table or figure. Please refer to the Sample Manuscript. The Journal reserves the right to safeguard its style and technical quality. Failure of authors to meet the manuscript submission requirements as given below may cause a delay in publication.
There are no page charges for publication in the NED University Journal of Research.

Manuscript Eligibility Criteria

A manuscript submitted to the NED University Journal of Research implies that it is an original and unpublished work and that it is not under consideration for publication elsewhere. The Editorial Board considers a work not eligible for publication if most of the contents of the paper are under consideration for publication in a journal, conference proceedings or book chapter. Abstracts or extended abstracts submitted to conferences do not constitute prior publication. Extended abstracts do not include tables and figures and are normally under 2000 words.

Formatting of Manuscript

The manuscript should be typewritten, double-spaced, single column on one side only of 8.5 x 11 in. (215 x 280 mm) paper with at least 1 in. (25.4 mm) margins. The reference and abstract must also be double spaced. Font style should be either times new roman or courier and the font size should be 12 pt. Hand written manuscript will not be accepted for review. Each page should be numbered beginning with the title page to facilitate review.

Length – the maximum number of words and word equivalents for a technical paper should normally be limited to 10,000 words. Although most topics can be covered within these limitations the Editor may waive these restrictions to encourage articles on topics that cannot be treated within these limitations. The authors must clearly provide a justification for longer manuscripts. As a typical guide a half-page figure or table [6 x 4 in. (150 x 100 mm)] should be counted as 250 words.

Language – papers must be clearly and concisely written in good English. The spellings should be UK spellings.

Equations – all equations should be typed clearly. Make sure that all characters and subscripts & superscripts are legible, distinguishable and clearly placed. Each equation should be identified by numbers in square brackets sequentially and placed flush with the left margin. An abbreviation of the word 'equation' must be used in the text in capital e.g. Eq. (1). A letter or symbol should be used only for one entity and be consistently used throughout the paper. Each variable must be defined either in the text or list of symbols. List of symbols is placed after the reference list. This section should also be typed double-spaced. Capital letters are placed before lowercase letters and Greek alphabets follow Roman alphabets.

References - References to published literature should be listed in the Vancouver (author-number) style at the end of the paper. They should reflect current state-of-technology and citied in the following style.
Journal:

[1] Alsyed HS, Alhozaimy MA. Ductility of Concrete Beams Reinforced with FRP Bars and Steel Fibers. J Compos Mater 1999;33(19):1792-1806.

Proceedings:

[2] Al-Salloum AY, Alsayed HS, Almusallam HT, Amjad AM. Some Design Considerations for Concrete Beams Reinforced by GFRP Bars. In: Saadatmanesh H, and Ehsani RM, Editors. Proceeding of First International Conference on Composites in Infrastructure. Tucson, Arizona: 1996. p. 318-331.

Book:

[3] Neville MA. Properties of concrete. England: Longman Scientific & Technical, England, 1981. p. 529-565.

Website:

[4] ConFibreCrete. Development of Guidelines for the Design of Concrete Structures, Reinforced, Prestressed or Strengthened with Advanced Composites, 2000 (updated 17 May 2000; accessed on 25 April 2005). Available from http://www.shef.ac.uk/~tmrnet

Thesis:

[5] Lodi SH. Reinforced Concrete Slab Elements Under Bending and Twisting Moments. PhD thesis. Heriot-Watt University, Edinburgh, 1997.

Tables– all tables should be in the portrait format. Each table should have a title and a number in Arabic numerals. The tables must be cited in the main text and capitalized in bold letters e.g. **Table 1**. The tables should be grouped together sequentially after the list of references in the order as they are cited in the text. The minimum text size for the tables is 8 point.

Figures and Illustrations – all figures should be in the portrait format. Recommended size of a figure is 4 x 5 in. (100 x 125 mm). The figures must be clear so as to be visible after reduction of size to suit the available Journal space. Each figure should have a title and a number in Arabic numerals. The figures must be cited in the main text and capitalized in bold letters e.g. **Fig. 1**. Figures should be grouped together sequentially at the end of the manuscript in the order as they are cited in the text.

© Copyright NED University of Engineering & Technology, Karachi - 75720, Pakistan